Behavioral/Systems/Cognitive

Chronic Nicotine Cell Specifically Upregulates Functional α4* Nicotinic Receptors: Basis for Both Tolerance in Midbrain and Enhanced Long-Term Potentiation in Perforant Path

Raad Nashmi,[1] Cheng Xiao,[1] Purnima Deshpande,[1] Sheri McKinney,[1] Sharon R. Grady,[2] Paul Whiteaker,[2] Qi Huang,[1] Tristan McClure-Begley,[2] Jon M. Lindstrom,[3] Cesar Labarca,[1] Allan C. Collins,[2] Michael J. Marks,[2] and Henry A. Lester[1]

[1]Division of Biology, California Institute of Technology, Pasadena, California 91125, [2]Institute of Behavioral Genetics, University of Colorado, Boulder, Colorado 80309, and [3]Department of Neuroscience, University of Pennsylvania, School of Medicine, Philadelphia, Pennsylvania 19104

Understanding effects of chronic nicotine requires identifying the neurons and synapses whose responses to nicotine itself, and to endogenous acetylcholine, are altered by continued exposure to the drug. To address this problem, we developed mice whose α4 nicotinic receptor subunits are replaced by normally functioning fluorescently tagged subunits, providing quantitative studies of receptor regulation at micrometer resolution. Chronic nicotine increased α4 fluorescence in several regions; among these, midbrain and hippocampus were assessed functionally. Although the midbrain dopaminergic system dominates reward pathways, chronic nicotine does not change α4* receptor levels in dopaminergic neurons of ventral tegmental area (VTA) or substantia nigra pars compacta. Instead, upregulated, functional α4* receptors localize to the GABAergic neurons of the VTA and substantia nigra pars reticulata. In consequence, GABAergic neurons from chronically nicotine-treated mice have a higher basal firing rate and respond more strongly to nicotine; because of the resulting increased inhibition, dopaminergic neurons have lower basal firing and decreased response to nicotine. In hippocampus, chronic exposure to nicotine also increases α4* fluorescence on glutamatergic axons of the medial perforant path. In hippocampal slices from chronically treated animals, acute exposure to nicotine during tetanic stimuli enhances induction of long-term potentiation in the medial perforant path, showing that the upregulated α4* receptors in this pathway are also functional. The pattern of cell-specific upregulation of functional α4* receptors therefore provides a possible explanation for two effects of chronic nicotine: sensitization of synaptic transmission in forebrain and tolerance of dopaminergic neuron firing in midbrain.

Key words: **nicotine addiction; GFP; knock-in mouse; nicotinic receptor; GABAergic; dopaminergic**

Introduction

Drugs of abuse induce changes such as tolerance, dependence, sensitization, and pleasure-seeking behavior. Chronic exposure to the drug may lead to changed levels and/or responsiveness of drug receptors themselves. For example, desensitization, down-regulation, and recycling of opioid receptors are thought to play key roles in opioid addiction (Waldhoer et al., 2004).

Chronic nicotine induces at least two phenomena that are challenging to explain in terms of changed receptor levels. The first is sensitization, both locomotor (Ksir et al., 1985; de Rover et al., 2004) and cognitive (Rezvani and Levin, 2001; Dani and Bertrand, 2007). In the human context, cognitive sensitization is epitomized by smokers' reports that they think better when they smoke; this anecdotal observation is confirmed by data that smokers who smoke nicotine cigarettes (but not nicotine-free cigarettes) display certain cognitive enhancements (Rusted and Warburton, 1992; Rusted et al., 1995). In the context of our studies on mice, rodents show more contextual fear conditioning if, 1 d after withdrawal from chronic nicotine, they receive an acute nicotine dose (Davis et al., 2005); also chronic nicotine produces better spatial working memory performance in the radial arm maze (Levin et al., 1990, 1996). The second phenomenon is tolerance to other effects such as reward; for instance, repeated nicotine treatment or nicotine self-administration results in chronic tolerance of mesolimbic dopamine release, which is closely associated with drug reward (Cadoni and Di Chiara, 2000; Di Chiara, 2000; Rahman et al., 2004).

Classical studies show that chronic nicotine exposure increases nicotinic acetylcholine receptor levels, but the increases differ among receptor subtypes and even vary among brain re-

Received Dec. 14, 2006; revised June 12, 2007; accepted June 14, 2007.

This work was supported by National Institutes of Health Grants DA-3194, DA-15663, DA-19655 (at Boulder); DA-09121, DA-17279, NS-11756 (at Caltech); DA-19375 (at both Boulder and Caltech); and NS-11323 (at the University of Pennsylvania); by the California Tobacco-Related Disease Research Project (Grant 12RT-0245); by Philip Morris USA/International at Caltech; by the Elizabeth Ross Foundation and National Alliance for Research on Schizophrenia and Depression (postdoctoral fellowships to R.N.); and by the W. M. Keck and Plum Foundations. We thank J. Drago for α4 knock-out mice. We thank V. Vargas, J. Wang, J. Silva, and S. Pease for excellent mouse husbandry; D. A. Dougherty, E. M. Schuman, J. L. Jankowsky, and J. Schwartz for comments on this manuscript; and B. N. Cohen, R. M. Drenan, C. Fonck, J. Miwa, R. Pantoja, and A. Tapper for discussions.

Correspondence should be addressed to Henry A. Lester, 156-29 Caltech, Pasadena, CA 91125. E-mail: lester@caltech.edu.

DOI:10.1523/JNEUROSCI.2199-07.2007

 0270-6474/07/278202-17$15.00/0

gions for the same subtype (Marks et al., 1983, 2004; Schwartz and Kellar, 1983; Pauly et al., 1996; Nguyen et al., 2004; McCallum et al., 2006). Data on isolated cells expressing nicotinic receptors also show that the upregulated receptors retain function and suggest that this upregulation arises primarily because more nicotinic receptors are assembled or stabilized in an easily activated state (Nashmi et al., 2003; Darsow et al., 2005; Kuryatov et al., 2005; Sallette et al., 2005; Vallejo et al., 2005). These changes may underlie mechanisms of sensitization. However, upregulation clearly disagrees with expectations that tolerance to nicotine is caused by fewer, or less functional, receptors. However, although the weight of evidence suggests that the upregulated receptors retain function (Nashmi et al., 2003; Nguyen et al., 2004; Darsow et al., 2005; Kuryatov et al., 2005; Sallette et al., 2005; Vallejo et al., 2005), it is still a viable hypothesis that most of the numerically upregulated receptors are actually desensitized, so that the upregulation would be masked or distorted by an overall decrease in sensitivity (Dani and Heinemann, 1996; Gentry and Lukas, 2002). The desensitization theory nicely explains tolerance, but it cannot directly explain sensitization.

This set of paradoxes, which we term the "upregulation dilemma," has led some researchers to suggest that nicotinic receptor upregulation is an epiphenomenon during chronic exposure to nicotine. Other signal transduction mechanisms, especially arising from Ca^{2+} influx through activated nicotinic acetylcholine receptors (nAChRs), apparently lead to adaptations in other proteins in addition to nAChRs (Chang and Berg, 2001; Ferrari et al., 2002; Brunzell et al., 2003; Marrero et al., 2004; Yeom et al., 2005; Marttila et al., 2006; Yamazaki et al., 2006b; Fornari et al., 2007). These adaptations, downstream from the receptors, could govern nicotine addiction at the cellular and circuit level (Koob et al., 2004; Laviolette and van der Kooy, 2004).

To assess the importance of receptor upregulation in the changes provoked by chronic nicotine, we asked whether upregulation can provide an explanation for chronic nicotine effects, both in the areas in forebrain thought to govern some simple aspects of cognition, as well as in the areas in midbrain thought to govern tolerance and reward. To monitor receptor changes, both numerically and functionally at a cellular level, we used an approach based on fluorescent receptors in knock-in mice. We studied receptors containing the α4 nicotinic receptor subunit (α4* receptors, primarily α4β2* receptors), because (1) these are among the most nicotine-sensitive subtypes (Luetje and Patrick, 1991), (2) these are also among those upregulated by chronic nicotine (Flores et al., 1992; McCallum et al., 2006), and (3) nicotine activation of these receptors is both necessary and sufficient for tolerance, sensitization, and reward behavior (Picciotto et al., 1998; Tapper et al., 2004; Maskos et al., 2005).

Materials and Methods

Mice. All experiments were conducted in accordance with the guidelines for care and use of animals provided by the National Institutes of Health, and protocols were approved by the Institutional Animal Care and Use Committee at the California Institute of Technology or the University of Colorado, Boulder. Mouse strains used in this study included α4YFP (see below), α4(Leu9′Ala) (Tapper et al., 2004), α4 knock-out (KO) (Ross et al., 2000), and GAT1-green fluorescent protein (GFP) (Chiu et al., 2002). Mice were kept on a standard 12 h light/dark cycle at 22°C and given food and water *ad libitum*. The α4YFP mice had a mixed Sv129/C57BL/6 background with one or more generations backcrossed to C57BL/6. Thus, all tissues studied were derived from mice with a mixed Sv129/C57BL/6 background, except that the slice experiments used inbred C57BL/6 mice.

α4YFP mouse construction. The strategy used to generate the α4YFP line adapts the procedures used to generate the previous Leu9′Ser line (Labarca et al., 2001; Tapper et al., 2004; Fonck et al., 2005) (see Fig. 1*A–D*). From previous work, we have in hand a 129/SvJ α4 genomic clone containing exon 5 and exon 6 with the L9′S mutation in the vector pKO Scrambler V907 (15.2 kb in length; Lexicon Genetics, The Woodlands, TX). A neomycin resistance cassette with a phosphoglycerate kinase promoter and polyadenylation signal flanked by loxP sites is present 166 bp downstream from exon 5 for positive selection. The diphtheria toxin A chain gene with an RNA polymerase II promoter has also been added to provide negative selection for random insertion.

A 4.1 kb cassette containing exon 5 and the L9′S mutation was removed from the pKO vector via digestion with *Spe*I and inserted into pBlueScript for modification (7.2 kb total length). The L9′S mutation was replaced with its wild-type (WT) codon by replacing an *Avr*II and *Sac*I fragment (5.7 kb) by enzyme digestion and ligation from a WT α4 genomic clone in Bluescript. According to our previous work, we found that the optimal insertion site for yellow fluorescent protein (YFP) was a *Bst*EII site in the M3–M4 cytoplasmic loop of α4 (Nashmi et al., 2003). There were two *Bst*EII sites in the 4.1 kb *Spe*I fragment inserted in pBlueScript, however. Therefore, a partial digestion was performed with *Bst*EII enzyme so that only one of the two sites was cut. YFP was cut from the previously published α4YFP cDNA construct with *Bst*EII (Nashmi et al., 2003), and then ligated to the 4.1 kb cassette in pBlueScript. The YFP insert also contained an immediately upstream hemagglutinin (HA)-epitope tag. Restriction analysis with *Bsr*GI and sequencing confirmed correct insertion orientation. The 4.1 kb exon 5 cassette was then removed by digestion with *Spe*I and ligated back into the α4(L9′S) knock-in construct, thus replacing the L9′S mutation with the WT L9′codon and inserting the YFP sequence. Clones were screened for correct orientation with restriction analysis using *Nsi*I enzyme and sequencing. The α4YFP knock-in construct (15.9 kb) was linearized with *Not*I, chloroform/phenol extracted, precipitated in ethanol-ammonium acetate at −20°C, and resuspended in sterile water in preparation for introduction into mouse embryonic stem cells (ES cells).

CJ7 mouse ES cells were electroporated with 25 μg of linearized knock-in construct. Four rounds of electroporation were performed using 7×10^7 ES cells per electroporation. After electroporation, each group of cells was plated on 10 cm dishes containing single layers of mitotically inactivated mouse primary fibroblasts. To select for recombinant clones, geneticin (G418) (180 μg/ml) was applied to ES cells 24 h after plating. Cell death was apparent 3 d after treatment. After 8 d of G418 treatment, 384 resistant colonies were picked and plated onto 96-well plates, grown for 72 h, trypsinized, and then split onto duplicate plates, one for freezing the other for screening. Correct recombinant colonies were screened for the presence of the neo cassette and YFP insert by a combination of PCR and automated sequence analysis. DNA for PCR and sequencing was isolated by applying lysis buffer (10 mM Tris, pH 7.5, 10 mM EDTA, 10 mM NaCl, 1% SDS, and 1 mg/ml proteinase K) to cells and incubating overnight at 60°C followed by ethanol precipitation. To confirm the correct position of the homologous recombination of the targeting construct within the genome and the insertion of YFP and neo cassette, ES cells were screened by PCR and sequencing. Two separate sets of PCRs were performed. One PCR included the forward primer (SEQS), 5′-GACCAACTGGACTTCTGGGAAAGTG-3′, and the reverse primer (SEQYFPAS), 5′-CTGTTGTAGTTGTACTCCAGCTTGTG-3′. The second PCR included the forward primer (SEQYFPS), 5′-CACAAGCTGGAGTACAACTACAAC-3′, and the reverse primer (S10L3′AS), 5′-CACTCCTACTGGTCTAGAGAGATG-3′. Karyotype analysis was used to assess chromosome number. Two positive clones with the highest percentage of proper chromosome number (90%) were selected for the subsequent round of electroporation.

Previous work with the Leu9′Ser mice has indicated that the presence of the neo cassette reduces expression of the target gene by approximately fourfold. To maximize expression of the mutated gene, we deleted the neo cassette. This was done by electroporating two clones of the neo-intact α4YFP ES cells with cytomegalovirus-Cre plasmid, leaving only a single 34 bp loxP. Electroporation was performed as described above. Cells were plated at a low density (600 cells/plate) onto 10 cm dishes containing single layers of mitotically inactivated mouse primary fibro-

blasts. A total of 178 colonies were picked and plated onto two 96-well plates, grown for 48 h, trypsinized, and split onto triplicate 96-well plates, one for freezing and two for screening. Clones were initially selected for neo cassette deletion by G418 (180 μg/ml) treatment. G418-sensitive clones were then further screened using a combination of PCR and automated sequencing. Primers were designed to anneal to a DNA sequence upstream of the 5′ loxP site while inside the YFP sequence (SEQYFPS), 5′-CACAAGCTGGAGTACAACTACAAC-3′, and downstream of the 3′ loxP site (SwaI/loxPAS), 5′-CAGGTGTTAGAATCATAGGGCTAG-3′. All neo-deleted clones were sequenced to confirm the presence of the YFP mutation and deletion of the neo cassette. Karyotype analysis was used to verify normal chromosome number. Two neo-deleted α4YFP clones were injected into C57BL/6 blastocysts, and chimeras were established. Chimeras were mated with wild-type animals and germline transmission was established as assessed by PCR analysis of tail DNA and sequence analysis. Primers used for genotyping included the following: A4XFPF, 5′-CAACCGCATGGACACAGCAGTCGAGAC-3′; A4XFPM, 5′-GCACAAGCTGGAGTACAACTACAACAGC-3′; A4XFP2R, 5′-CTCAGTCAGGGAAGCAGCTCCATCTTG-3′.

RT-PCR. Total RNA was extracted from combined fresh frozen thalamus and ventral midbrain tissue from heterozygous (Het) and WT α4YFP mice (RNeasy Protect number 74124; Qiagen, Valencia, CA). The first-strand cDNA was synthesized using SuperScript II reverse transcriptase (Invitrogen, Carlsbad, CA) with the specific primer A4RTPCRAS, 5′-GATCATACCAGCCAACCATGGAG-3′. PCR amplification of α4YFP nAChR was done using the following primers: A4XFPF, 5′-CAACCGCATGGACACAGCAGTCGAGAC-3′; A4XFPM, 5′-GCACAAGCTGGAGTACAACTACAACAGC-3′; A4RTPCRAS, 5′-GATCATACCAGCCAACCATGGAG-3′.

Acetylcholine-stimulated $^{86}Rb^+$ efflux. Nicotine-stimulated $^{86}Rb^+$ efflux from thalamic and cortical synaptosomes of WT, Het, and homozygous (Hom) α4YFP mice was measured as described previously (Marks et al., 1999). Cortex and thalamus (excluding habenula) were dissected from adult mice killed by cervical dislocation. Tissue was homogenized by hand in 1 ml of ice-cold 0.32 M sucrose buffered to pH 7.5 with HEPES using a glass/Teflon tissue grinder. After homogenization, the grinder was rinsed three times with 0.5 ml of buffered sucrose solution. A crude synaptosomal pellet was obtained by centrifugation at 12,000 × *g* for 20 min. After removal of the sucrose, each pellet was resuspended in 0.35 ml (thalamus) or 0.8 ml (cortex) of load buffer (in mM: 140 NaCl, 1.5 KCl, 2 $CaCl_2$, 1 $MgSO_4$, 25 HEPES, and 22 glucose) and placed on ice until incubation with ^{86}RbCl. Thalamic and cortical synaptosomes were incubated with 4 μCi of $^{86}Rb^+$ for 30 min in a final volume of 35 μl of load buffer, after which samples were collected by gentle filtration onto a 6-mm-diameter Gelman-type A/E glass filter and washed once with 0.5 ml of load buffer. Filters containing the synaptosomes loaded with $^{86}Rb^+$ were transferred to a polypropylene platform and superfused for 5 min with effluent buffer (in mM: 135 NaCl, 1.5 KCl, 5 CsCl, 2 $CaCl_2$, 1 $MgSO_4$, 25 HEPES, 22 glucose, 50 nM tetrodotoxin, and 0.1% bovine serum albumin). A peristaltic pump applied buffer to the top of the synaptosome containing filter at a rate of 2 ml/min, and a second peristaltic pump set at a faster flow rate of 3 ml/min removed buffer from the bottom of the platform. The greater speed of the second pump prevented pooling of buffer on the filter. Effluent buffer was pumped through a 200 μl Cherenkov cell and into a β-Ram detector (IN/US Systems, Tampa, FL). Radioactivity was measured for 3 min with a 3 s detection window providing 60 data points for each superfusion. Each aliquot was stimulated by 1 of 10 different acetylcholine (ACh) concentrations, with a 5 s exposure for each concentration.

Neurotransmitter release. After a mouse was killed by cervical dislocation, its brain was removed and placed immediately on ice. The striatal and hippocampal tissue dissected from each mouse was homogenized in 0.5 ml of ice-cold 0.32 M sucrose buffered with 5 mM HEPES, pH 7.5. A crude synaptosomal pellet was obtained by centrifugation at 12,000 × *g* for 20 min at 4°C. The pellets were resuspended in 0.8 ml of "uptake buffer" (in mM: 128 NaCl, 2.4 KCl, 3.2 $CaCl_2$, 1.2 KH_2PO_4, 1.2 $MgSO_4$, 25 HEPES, pH 7.5, 10 glucose). For [^{3}H]dopamine uptake, the buffer was supplemented with 1 mM ascorbic acid and 0.01 mM pargyline. For [^{3}H]GABA uptake, the buffer was supplemented with 1 mM aminooxyacetic acid.

For [^{3}H]GABA uptake, the crude hippocampal synaptosomes were incubated for 10 min at 37°C. [^{3}H]GABA and unlabeled GABA were then added to final concentrations of 0.1 and 0.25 μM, respectively, and the suspension was incubated for another 10 min.

For [^{3}H]dopamine uptake, striatal synaptosomes were incubated at 37°C in uptake buffer for 10 min before addition of 0.1 μM [^{3}H]dopamine and the suspension was incubated for an additional 5 min (Grady et al., 1997). Because ACh was used as the agonist, the synaptosomes were treated with diisopropyl fluorophosphate (10 μM) during the last 5 min of the uptake procedure.

All release experiments were conducted at room temperature using methods described previously (Grady et al., 1997, 2001). In brief, after ^{3}H-neurotransmitter uptake was complete, aliquots of synaptosomes (80 μl) were distributed onto filters and perfused with perfusion buffer [uptake buffer containing 0.1% bovine serum albumin, 1 μM atropine, and either 10 μM nomifensine for [^{3}H]dopamine release or 0.1 μM NNC-711 [1-(2-(((diphenylmethylene)amino)oxy)ethyl)-1,2,5,6-tetrahydro-3-pyridinecarboxylic acid hydrochloride] for [^{3}H]GABA release] at 0.7 ml/min for 10 min before fractions were collected. Fractions were collected every 10 s into 96-well plates using a Gilson FC204 fraction collector (Gilson, Middleton, WI). Optiphase Supermix Scintillation Fluid (150 μl) was added to each well, and radioactivity was determined using a 1450 MicroBeta Trilux Scintillation Counter (PerkinElmer Life Sciences, Boston, MA). Instrument efficiency was 40%.

Basal $^{86}Rb^+$ efflux or neurotransmitter release was calculated by nonlinear least-squares curve fit of the samples before and after the ACh-stimulated peak to a first-order equation: $C_t = C_0 \times e^{-kt}$, where C_t is baseline counts at time t, C_0 is baseline counts at $t = 0$, and k is the first-order constant for basal efflux or release. ACh-stimulated response was calculated as the difference between the actual sample counts after ACh stimulation and the estimated basal counts. ACh-stimulated response at each concentration was normalized by dividing by the calculated basal efflux; thus, ACh-stimulated $^{86}Rb^+$ efflux or transmitter release is expressed as the response relative to baseline. EC_{50} values were calculated using the following Hill equation: $E_{ACh} = E_{max} \times [ACh]^{nH}/([ACh]^{nH} + EC_{50})$, where E_{ACh} is the response measured after stimulation with ACh concentration [ACh], and n_H is the Hill coefficient. Concentration–response experiments were fitted with one Hill equation for transmitter release experiments and the sum of two Hill equations for $^{86}Rb^+$ efflux experiments.

^{125}I-Epibatidine binding. Epibatidine binding was used for quantitating nicotinic receptor levels in various brain regions of WT, Het, and Hom α4YFP mutant mice as described previously (Whiteaker et al., 2002). Tissue was collected from the thalamus, cerebral cortex, hippocampus, and striatum, and homogenized in ice-cold 0.1× binding buffer (in mM: 14.4 NaCl, 0.2 KCl, 0.2 $CaCl_2$, 1 $MgSO_4$, and 2 HEPES, pH 7.5). Homogenates were washed three times by centrifugation (12,000 × *g*; 15 min; 4°C) and resuspension into 0.1× binding buffer and stored at −70°C. For saturation binding experiments, ^{125}I-epibatidine concentrations were varied between 3 and 400 pM. The 200 pM ^{125}I-epibatidine (a saturating concentration) was used in inhibition binding experiments. Cytisine inhibition of ^{125}I-epibatidine was measured using drug concentrations of 0.1–3000 nM plus a no-drug control. The amount of membrane protein added was chosen to produce maximum ligand binding to the tissue of <1000 Bq/well (<5% of total ligand added, minimizing the effects of ligand depletion) and a minimum of 350 Bq of specific binding. Membranes were incubated for 2 h at 22°C in 30 μl of binding buffer. Nonspecific binding was determined in the presence of 1 mM (−)nicotine tartrate and fell in the range of 20–50 Bq. Incubations were terminated by filtration onto Gelman GF/F fiber filters using a cell harvester, followed by six washes with ice-cold binding buffer. Bound ligand was measured at 80–85% efficiency using a Packard Cobra gamma counter (PerkinElmer). Specific binding was calculated for each region from every animal by subtraction of the relevant nonspecific binding value. Saturation binding parameters were calculated by fitting data to the following Hill equation: $B = B_{max}L^n/(L^n + K_D{}^n)$, where B is the binding at the free ligand concentration L, B_{max} is the maximum number of binding sites, K_D is the equilibrium binding constant, and n is the Hill coefficient. Inhibition of ^{125}I-epibatidine binding was calculated using a

two-site fit: $B = B_1/(1 + (I/IC_{50\text{-}1})) + B_2/(1 + (I/IC_{50\text{-}2}))$, where B was ligand bound at inhibitor concentration I, and B_1 and B_2 represent ^{125}I-epibatidine binding to sites sensitive to cytisine inhibition with $IC_{50\text{-}1}$ and $IC_{50\text{-}2}$ (cytisine-sensitive and cytisine-resistant sites, respectively).

^{125}I-mAb 299 labeling. Three mice of each genotype were killed by cervical dislocation and decapitated, and whole brains were removed. Brains were rapidly frozen in isopentane (−35°C, 10 s) and stored, wrapped in aluminum foil, at −70°C until sliced. Coronal tissue sections (14 μm thick) were obtained using a Leica (Nussloch, Germany) CM 1850 cryostat/microtome, and thaw mounted onto SuperFrost glass slides (Fisher Scientific, Pittsburgh, PA). Sections were stored, desiccated, at −70°C until analyzed.

^{125}I-mAb autoradiography was performed as described (Whiteaker et al., 2006). Sections were allowed to equilibrate to room temperature, and then rehydrated for 15 min in 100 mM NaCl, 10 mM sodium phosphate buffer, pH 7.5 (PBS). The hydrated sections were then overlaid with ^{125}I-mAb 299 (0.3 nM) in PBS supplemented with 10 mM NaN_3, 10% (v/v) normal rat serum, and 5% (w/v) protease-free bovine serum albumin, and incubated for 48 h (humidified chambers, 4°C). A set of α4 KO sections was incubated in parallel, for each experiment, to define nonspecific ^{125}I-mAb 299 labeling. Incubated sections were washed in four changes of PBS (30 min each; 22°C), and then air-dried and desiccated overnight under vacuum before exposure to Super Resolution phosphorimaging screens (PerkinElmer Life Sciences; 2–4 d exposure). Images were collected using a Packard Cyclone system (PerkinElmer Life Sciences) and quantitated using the associated OptiQuant software. Regions were identified by reference to an atlas (Paxinos and Franklin, 2004). Generally, six separate samples were taken for each region in each mouse (exceptions were made for very small regions such as the interpeduncular nucleus, where fewer than six samples were available). For large regions such as striatum, thalamus, and cortex, samples were taken throughout the rostral–caudal span of the structure, to ensure that regional heterogeneity did not influence the results. Labeling intensity was measured in terms of digital light units per square millimeter. Specific ^{125}I-mAb 299 labeling in each region was defined by subtracting labeling in the corresponding region of α4 KO brain sections. Studies on α4 knock-out mice with this procedure show the specificity of our method (Whiteaker et al., 2006).

Chronic nicotine administration. Chronic nicotine or saline was administered to mice using miniosmotic pumps (model 2002; Alzet, Cupertino, CA). On the day of pump implantation, saline or (−)-nicotine hydrogen tartrate (Sigma, St. Louis) was prepared freshly and loaded into the pump to deliver nicotine at 2 $mg \cdot kg^{-1} \cdot h^{-1}$ [which provides maximal nAChR upregulation (McCallum et al., 2006) and also provides a blood concentration of 590 nM (Marks et al., 2004), near the peak concentration in the blood of smokers] or 0.4 $mg \cdot kg^{-1} \cdot h^{-1}$ with a flow rate of 0.5 μl/h. Surgery was identical with the description of telemetry probe implantation.

Hot plate. For antinociception experiments, a hot plate was set at 55°C. A baseline response was determined for each mouse and a cutoff time of 60 s was instituted. The nociceptive time point was indicated by jumping, paw licking, or rapid thumping of the paw, at which point the mouse was immediately removed from the hot plate. Mice were allowed to recover for one-half of an hour before the mouse was tested again but with subcutaneous injection with one dose of (−)-nicotine at either 0, 1, or 1.5 mg/kg (prepared in saline). Five minutes after the injection, the mouse was placed again on the hot plate, and the time was noted for reaction to the nociceptive stimuli of the hot plate. Antinociceptive response was measured as percentage of maximal possible effect (%MPE) (Marubio et al., 1999). %MPE = [(test − control)/(cutoff − control)] × 100.

Sample preparation for immunohistochemistry and spectral imaging. At day 10 of chronic infusion of saline or nicotine via miniosmotic pumps, mice were anesthetized with halothane (2-bromo-2-chloro-1,1,1-trifluorothane) and subjected to cardiac perfusion first with 20 ml of PBS, pH 7.6, with heparin, second with 30 ml of 4% paraformaldehyde in PBS, pH adjusted to 7.6 with Na_2HPO_4, and finally with 20 ml of 5% sucrose in PBS, pH 7.6. Thus, animals were perfused and fixed while the miniosmotic pumps were still active. All solutions were on ice. Brains were dissected and then incubated in 30% sucrose in PBS, pH 7.6, for 3 d at 4°C. The brains were embedded in OCT medium (Tissue-Tek, Torrance, CA) and rapidly frozen in 2-methylbutane on dry ice. Coronal and sagittal sections were sliced by cryostat at 30 μm and mounted on slides. Slides with mounted brain sections were stored at −20°C. Before imaging, slices were rinsed with PBS, pH 7.6, and mounted with Mowiol and coverslipped.

Immunohistochemistry. Brain sections on slides were rinsed twice for 10 min with PBS, pH 7.6, and then permeabilized with 0.25% Triton X-100 in PBS for 5 min. Cultures were rinsed twice for 10 min with PBS and blocked with 10% donkey serum (Jackson ImmunoResearch, West Grove, PA) in PBS for 30 min. The primary antibody was diluted in 3% donkey serum in PBS and incubated for 1 h at 37°C. Brain sections were then washed three times for 5 min with PBS. The secondary antibody was diluted in 3% donkey serum in PBS and incubated for 1 h at 37°C. The incubation and rinsing steps were repeated for second primary antibody labeling when triple-label immunohistochemistry was performed. Finally, brain sections were washed three times for 5 min with PBS and mounted with Mowiol and coverslipped.

The following primary and corresponding secondary antibodies and their dilutions were used in this study: rabbit anti-MAP2 (microtubule-associated protein 2) polyclonal antibody at 1:50 (AB5622; Chemicon, Temecula, CA), CY5-conjugated donkey anti-rabbit (Jackson ImmunoResearch) at 1:100, mouse anti-GAD67 monoclonal antibody at 1:50 (MAB5406; Chemicon), CY5-conjugated donkey anti-mouse (Jackson ImmunoResearch) at 1:100, rabbit anti-tyrosine hydroxylase (Pel-Freez, Rogers, AR) at 1:50, CY5-conjugated donkey anti-rabbit (Jackson ImmunoResearch) at 1:100, sheep anti-tyrosine hydroxylase polyclonal (AB1542; Chemicon), and Cy3-conjugated donkey anti-sheep IgG (Jackson ImmunoResearch).

Spectral confocal imaging. For quantification of α4YFP fluorescence, images were collected from either of two microscopes equipped with spectrally resolved multiple detector systems. Each pixel of the *X–Y* image has complete spectral emission data, comprising the λ stack. With an inverted LSM 510 Meta laser-scanning confocal microscope (Zeiss) using a Fluar 20×, 0.75 numerical aperture (NA) oil immersion objective (Dickinson et al., 2001; Lansford et al., 2001; Nashmi et al., 2005), images were collected at wavelengths between 495 and 602 nm with bandwidths of 10.7 nm during excitation of YFP with the 488 nm line of an argon laser (1–10%; 23–114 μW). Pinhole was 1.68 Airy units and a *Z* resolution of ~2.9 μm. Images were collected at a 12-bit intensity resolution over 1024 × 1024 pixels at a pixel dwell time of 6.4 μs.

Other spectral images were taken, with excitation at 488 nm, with an inverted Nikon C1si laser-scanning confocal microscope (Nikon, Tokyo, Japan) over 512 × 512 pixels at 12-bit intensity resolution using a 60× plan apochromat water (1.2 NA) objective. The pinhole was set to a nominal diameter of 61.3 μm. The GAT1-GFP images were excited by a 440 nm modulated diode laser at 20% power. λ stacks of images were acquired at wavelengths between 479 and 634 nm, at 5 nm steps.

In all cases, detector gains and laser attenuators were adjusted to lie within the linear range of the detector. The output of the appropriate laser was calibrated at each session with a power meter.

The α4YFP knock-in mice present the advantage that the fluorescent moiety appears at WT levels rather than overexpressed levels, but this limits the fluorescence signal. Some brain regions had significant amount of autofluorescence. We used the capabilities of spectral imaging to deconvolve specific YFP fluorescence from background autofluorescence at each pixel using a linear unmixing algorithm based on the spectral signatures of YFP and autofluorescence created from reference λ stack images of HEK293T cells expressing soluble YFP and a fixed brain section from WT littermates of α4YFP mice, respectively (Dickinson et al., 2001; Lansford et al., 2001; Nashmi et al., 2005).

Image analysis of cell counts, mean intensities, and area measurements were done with ImageJ, version 1.37, software (National Institutes of Health, Bethesda, MD; http://rsb.info.nih.gov/ij/). Details of analyses of each region are shown in Tables 1 and 2. To calculate the mean spectrally unmixed YFP fluorescence from a particular brain region from a Hom or Het mouse, the corresponding spectrally unmixed residual background fluorescence from the same brain region of a WT mouse was subtracted.

Calcium imaging in cultured ventral midbrain neurons. Changes in

Table 1. α4YFP intensities in ventral midbrain neurons

					Cell-based measurements (no. of cells)			
					Saline (6 mice)		Nicotine (6 mice)	
	Saline	Nicotine	Nicotine, % of saline	*p* value	Total	$\alpha4^+$	Total	$\alpha4^+$
VTA (TH^+)	826 ± 22	902 ± 23	109 ± 3	NS	640	610	655	648
VTA (GAD^+)	268 ± 25	363 ± 18	136 ± 7	0.002	73	67	100	99
SNC (TH^+)	1052 ± 23	1117 ± 25	106 ± 2	NS	612	610	581	579
SNR (GAD^+)	503 ± 17	735 ± 18	146 ± 4	<0.001	256	254	237	237

Measurements of α4YFP fluorescence in various brain regions and changes with chronic nicotine (2 mg · kg^{-1} · h^{-1} for 10 d). Procedures were applied to each of the six mice in each group. Unless otherwise stated, analyses were performed on one brain section per mouse. In VTA, all TH^+ or GAD^+ somata were measured. In SNC, TH^+ or GAD^+ cell bodies were measured in one of two lobes. NS, Not significant; no., number.

Table 2. α4YFP intensities in various brain regions

					Area-based measurements (μm^2)	
	Saline	Nicotine	Nicotine, % of saline	*p* value	Saline (6 mice)	Nicotine (6 mice)
Superior colliculus	195 ± 20	262 ± 21	134 ± 12	0.027	11×10^5	12×10^5
Medial habenula	669 ± 55	749 ± 24	112 ± 4	NS	1.7×10^5	1.6×10^5
Fasciculus retroflexus	599 ± 86	673 ± 41	112 ± 7	NS	2.8×10^5	1.8×10^5
Interpeduncular nucleus	1216 ± 71	984 ± 38	81 ± 3	0.01	3.0×10^5	2.3×10^5
Perforant path	287 ± 8	555 ± 7	194 ± 2	<0.001	5.2×10^5	4.1×10^5
Nucleus accumbens	318 ± 25	357 ± 18	112 ± 6	NS	21×10^5	21×10^5
Caudate putamen	353 ± 11	417 ± 15	118 ± 4	0.002	31×10^5	29×10^5
Cerebral cortex	273 ± 18	236 ± 16	86 ± 6	NS	13×10^5	11×10^5
Anterior cingulate cortex	299 ± 21	407 ± 23	136 ± 8	<0.001	7.2×10^5	7.5×10^5
Thalamic DLG nucleus	840 ± 71	928 ± 38	111 ± 4	NS	10×10^5	11×10^5

Measurements of α4YFP fluorescence in various brain regions and changes with chronic nicotine (2 mg · kg^{-1} · h^{-1} for 10 d). Procedures were applied to each of the six mice in each group. Unless otherwise stated, analyses were performed on one brain section per mouse. Area-based measurements were conducted as follows: superior colliculus, four regions, 150 μm most dorsal aspect; medial habenula, lower two-thirds of each of two lobes; fasciculus retroflexus, two cross sections; interpeduncular nucleus, two sections; perforant path, four regions in the lower limbs of the medial perforant path; nucleus accumbens, two regions; caudate putamen, four regions in the dorsal aspect; cerebral cortex, two regions in layers 2–5 in the barrel cortex somatosensory area; anterior cingulate cortex, two regions 75 μm from midline in two brain sections per mouse; and thalamic dorsolateral geniculate (DLG) nucleus, one region in each of the two nuclei.

$[Ca^{2+}]_i$ were measured in ventral midbrain neuronal cultures using the ratiometric fura-2 method as described previously (Nashmi et al., 2003; Tapper et al., 2004; Fonck et al., 2005). Ventral midbrain tissue [including the substantia nigra (SN) and ventral tegmental area (VTA)] obtained from embryonic day 14 embryos was digested with 1 mg/ml papain, and cells were mechanically separated by gentle pipetting. Cells were plated onto 35 mm dishes with glass coverslip bottoms in Neurobasal culture medium containing 2% B27 supplement, 0.5 mM Glutamax, and 5% horse serum, all obtained from Invitrogen. Cell cultures were kept in a temperature-, humidity-, and CO_2/O_2-controlled incubator. Measurements were made at 28–35 d in culture. For experiments with chronic nicotine, 10 nM was applied for 3 d and removed ~1 h before the imaging experiments. During this 1 h period, cells were loaded with 1.25 μM fura-2 AM (Invitrogen) in a 0.01% pluronic acid solution for 30 min at room temperature (22 ± 2°C) and in the dark. During experiments, cultures were continually perfused with an extracellular solution (in mM: 150 NaCl, 10 HEPES, 10 glucose, 4 KCl, 2 $CaCl_2$, and 2 $MgCl_2$). Various channel blockers to suppress nonspecific responses were included in the extracellular solution as follows (in μM): 0.5 TTX (voltage-gated Na^+ channels), 0.5 atropine (muscarinic receptors), 10 CNQX (AMPA and kainate receptors), 20 bicuculline ($GABA_A$ receptors), 50 AP-5 (NMDA receptors), and 0.01 methyllycaconitine (MLA) (α7 receptors). Ascorbic acid at 1 mM was also added to the extracellular solution to protect neurons from photodamage. Imaging was performed with an inverted fluorescence microscope (IX71; Olympus, Melville, NY) using a 40× oil-immersed objective (UApo/340; 1.35 NA). To generate ratiometric estimates of $[Ca^{2+}]_i$, pairs of images were obtained with alternate excitation wavelengths of 340/380 nm and emission wavelength of 510 nm. A U-tube connected to a pipette, placed ~0.5 mm away from the targeted cell population, was used to deliver nicotine. Nicotinic receptors desensitize at agonist concentrations too low to cause appreciable activation; therefore, between applications, negative pressure was maintained on the U-tube to prevent nicotine from leaking out of the pipette. Nicotine was applied onto cultured cells when solution flow in the U-tube was momentarily (2 s) reversed by stopping outflow with a computer-controlled valve. Images were captured with a 16 bit CCD camera (Cascade 650; Photometrics, Tucson, AZ) and analyzed with Slidebook 4.1 imaging software (Intelligent Imaging Innovations, Denver, CO).

Whole-cell patch-clamp electrophysiology of cultured ventral midbrain-neurons. Cultures were prepared and maintained as described in the fura-2 experiments. Whole-cell recordings were performed with glass electrodes (2–5 MΩ) filled with an internal solution [in mM: 88 KH_2PO_4, 4.5 $MgCl_2$, 0.9 EGTA, 9 HEPES, 0.4 $CaCl_2$, 14 creatine phosphate, 4 Mg-ATP, and 0.3 GTP (Tris salt), pH 7.4 with KOH] (Nashmi et al., 2003; Fonck et al., 2005). Channel blockers to suppress nonspecific responses were included in the extracellular solution (in μM: 0.5 TTX, 0.5 atropine, 10 CNQX, 20 bicuculline, 50 AP-5, and 0.01 MLA). Recordings were made using an Axopatch 1D (Molecular Devices, Union City, CA) amplifier, low-pass filtered at 2–5 kHz, and digitized on-line at 20 kHz (pClamp 8; Molecular Devices). The membrane potential was held at −70 mV. The 3 μM ACh test pulses lasting 250 ms were delivered with a two-barrel glass theta tube pulled from borosilicate tubing and connected to a piezoelectric translator (LSS-3100; Burleigh Instruments, Fishers, NY).

Patch-clamp electrophysiology on midbrain slices. The patch-clamp experiments were conducted blind to the contents of the osmotic minipumps (nicotine vs saline) until the conclusion of recording from each group of implanted mice. P30–P38 mice were deeply anesthetized with sodium pentobarbital (40 mg/kg). Then, cardiac perfusion was performed using ice-cold glycerol-based artificial CSF (gACSF), containing 252 mM glycerol, 1.6 mM KCl, 1.2 mM NaH_2PO_4, 1.2 mM $MgCl_2$, 2.4 mM $CaCl_2$, 18 mM $NaHCO_3$, and 11 mM glucose, and oxygenated with 95%O_2/5%CO_2. After decapitation, the brain was removed and kept in gACSF (0–4°C), and was cut into 250–300 μm thick slices in the coronal plane (DTK-1000; Microslicer; Ted Pella, Redding, CA). The slices were allowed to recover for at least 1 h in regular artificial CSF (aCSF), containing 126 mM NaCl, 1.6 mM KCl, 1.2 mM NaH_2PO_4, 1.2 mM $MgCl_2$, 2.4 mM $CaCl_2$, 18 mM $NaHCO_3$, and 11 mM glucose, and oxygenated with 95% O_2/5% CO_2.

A single slice was transferred to the 0.8 ml recording chamber. Throughout the experiments, the bath was continually perfused with aCSF (1.5–2.0 ml/min). Cells were visualized with an upright microscope (BX 50WI; Olympus) and near-infrared illumination. The patch elec-

trodes had a resistance of 5–8 MΩ when filled with pipette solution: 135 mM potassium gluconate, 5 mM EGTA, 0.5 mM $CaCl_2$, 2 mM $MgCl_2$, 10 mM HEPES, 2 mM Mg-ATP, and 0.1 mM GTP, pH adjusted to 7.2 with Tris base, osmolarity adjusted to 280–300 mOsm with sucrose. Whole-cell current-clamp was performed at 32°C with a MultiClamp 700B amplifier (Molecular Devices), a Digidata 1200A A/D converter, and pCLAMP 9.2 software (Molecular Devices). Data were sampled at 10 kHz and filtered at 2 kHz. The junction potential between the patch pipette and the bath solution was nulled just before gigaseal formation.

We verified the putative GABAergic neurons in the substantia nigra pars reticulata (SNR) and putative dopaminergic neurons in the substantia nigra pars compacta (SNC) (supplemental Fig. S6, available at www.jneurosci.org as supplemental material), according to generally accepted criteria (Lacey et al., 1989; Wooltorton et al., 2003): (1) narrow spikes in putative SNR GABAergic neurons, broad spikes in putative SNC dopaminergic neurons (supplemental Fig. S6*A*, available at www.jneurosci.org as supplemental material); (2) rapid firing in putative SNR GABAergic neurons, but slow firing in putative SNC dopaminergic neurons (supplemental Fig. S6*B*, available at www.jneurosci.org as supplemental material); (3) putative SNC dopaminergic neurons, but not putative SNR GABAergic neurons, express hyperpolarization induced cationic current (I_h) (supplemental Fig. S6*C*, available at www.jneurosci.org as supplemental material). In addition, in select experiments putative SNR GABAergic neurons and putative SNC dopaminergic neurons were respectively inhibited or disinhibited by DAMGO (Tyr-D-Ala-Gly-MePhe-Gly-ol) (1 μM), a μ-opioid receptor agonist; and putative SNC dopaminergic neurons, but not putative SNR GABAergic neurons (supplemental Fig. S6*D*, available at www.jneurosci.org as supplemental material), are inhibited by quinpirole (0.2 μM), a D_2/D_3 receptor agonist (Lacey et al., 1989; Wooltorton et al., 2003) (supplemental Fig. S6*E*, available at www.jneurosci.org as supplemental material). Given the good agreement between these criteria and the localization of these neurons (SNC vs SNR), we drop the term "putative," and subsequently, neurons were routinely characterized by location and spike duration.

To examine the function of nAChRs in SNR GABAergic neurons, 1 μM nicotine was focally puffed (5 s), using a picospritzer driven pipette attached to a piezoelectric translator (Tapper et al., 2004). The pipette was moved within 20 μm of the recorded cell over a period of 250 ms starting 300 ms before drug application. Nicotine was then puffed at 10–20 psi for 5 s. Fifty milliseconds after the puff, the glass pipette was retracted over a period of 250 ms. For dopaminergic recordings of nicotinic responses, because we could not determine the connectivity between GABAergic to dopaminergic neurons, it was inappropriate to use a focal drug applicator such as a picospritzer. Therefore, on recording of dopaminergic neurons, nicotine (1 μM) was bath applied for 5 min. This enabled nicotinic receptors to be activated on all GABAergic and dopaminergic neurons within the slice.

Long-term potentiation electrophysiology. Adult Hom α4YFP mice (2–3 months), treated with saline or nicotine for 10 d, were killed by cervical dislocation, and the brain was rapidly removed (<50 s) and placed in aerated (95% O_2/5% CO_2) ice-cold aCSF of the following composition (in mM): 124 NaCl, 3 KCl, 2.4 $CaCl_2$, 1.3 $MgSO_4$, 1.25 NaH_2PO_4, 26 $NaHCO_3$, and 10 glucose. After 4 min, the brain was hemisected and glued with cyanoacrylate glue dorsal side down and rostral side closest to the blade. Horizontal sections (400 μm) of the hippocampus were made with a vibratome (DSK Microslicer; model DTK-1000; Ted Pella) and allowed to recover for >1 h at room temperature. The slice was transferred to a submersion chamber (catalog #65-0073 and 65-0074; Harvard Apparatus, South Natick, MA) maintained at 32°C. The $GABA_A$ receptor blocker, bicuculline (10 μM), was added to the aerated aCSF during recording to relieve the strong GABAergic inhibition of the dentate gyrus (Colino and Malenka, 1993; Yun et al., 2005). Thus, brain tissue was removed from contact with the miniosmotic pump for periods of 2–8 h.

Stimulation of the medial perforant path was provided by bipolar stimulating electrodes fabricated from Formvar-coated Nichrome wires (50 μm bare diameter; catalog #762000; A-M Systems, Carlsborg, WA). Stimulating and recording electrodes were positioned in the suprapyramidal limb of the dentate gyrus in the middle one-third of the molecular layer to stimulate and record dendritic field EPSPs (fEPSPs). Recording electrodes (2–6 MΩ) were pulled from borosilicate pipettes (catalog #1B150F-4; WPI, Sarasota, FL) and filled with aCSF. Stimulating electrodes were placed ~200 μm from recording electrodes. Responses were recorded on an Axoclamp-2A amplifier (Molecular Devices), amplified 1000×, low-pass filtered at 3 kHz, and digitized at 10 kHz. An input–output relation for fEPSP slope was measured by varying the stimulus intensity (5–100 μA; 100 μs duration). The stimulus intensity that elicited 40% of the maximal slope was applied as test pulses and tetanic trains during long-term potentiation (LTP) experiments. Paired-pulse stimuli with a 50 ms interval were applied to check for fEPSP paired-pulse inhibition, indicating that stimulating and recording electrodes were located in the medial perforant path (Colino and Malenka, 1993; Yun et al., 2005). A steady baseline of fEPSP slopes was recorded for 20 min with a stimulation rate of 1 in 30 s. LTP was induced by three trains of 100 Hz, each 1 s in duration, at 4.5 min intervals. Responses were recorded thereafter for a period of 60 min. The magnitude of LTP was measured by averaging the percent increase of the fEPSP slope compared with baseline at 40–60 min after tetanic stimuli.

Statistical analysis. All values are reported as mean ± SEM. Significant differences (at $p < 0.05$) were determined between two groups using a *t* test for continuous data meeting parametric assumptions of normality and equal variance. Otherwise, the Mann–Whitney rank sum test was used for nonparametric data.

Results

We created a knock-in mouse strain whose α4 subunits are replaced by subunits containing yellow fluorescent protein (α4YFP subunits), which was inserted in-frame within the M3–M4 cytoplasmic loop of α4 (Nashmi et al., 2003). Previous data in transfected systems show that receptor function remains unaffected by this insertion (Nashmi et al., 2003); the knock-in strategy now places the α4YFP subunit under the control of the same promoters, enhancers, and trafficking mechanisms as WT α4 subunits, and provides cellular and subcellular resolution in the normal physiological milieu of the intact animal.

Characterizing the α4YFP mice: normal nicotinic receptor function

We proceeded to quantify the relative amount of α4 nAChR subunits in various brain regions. Figure 1 displays a series of montages of confocal images of a coronal brain section showing the overall distribution of α4 at the level of the hippocampus/thalamus (Fig. 1*E*; bregma, −1.58). We imaged λ stacks over a spectral range (supplemental Fig. S1, available at www.jneurosci.org as supplemental material), enabling us to isolate specific YFP fluorescence from autofluorescent background using reference spectra of YFP (cells transfected with soluble YFP) and autofluorescence (a fixed brain slice of a wild-type mouse). Summarizing data from 16 different brain regions in WT, Het, and Hom mice, the highest level of α4 expression was in the medial habenula, followed by the thalamus, SNC, and the interpeduncular nucleus. Moderate levels of α4 expression were found in the superior colliculus, cerebral cortex, retrosplenial granular cortex, and subiculum. This pattern agrees well with previous data (Swanson et al., 1987; Marks et al., 1992; Whiteaker et al., 2006). When α4YFP fluorescence is totaled for these 16 brain regions, the Het mouse brain fluorescence is approximately one-half (45%) that of Hom, consistent with straightforward gene dosage.

Detailed analyses of expression in ventral midbrain and in hippocampus are presented below (see Figs. 3–7); here, we present a survey of other areas. Most of the thalamus expressed strong α4YFP fluorescence (Fig. 1*E*). α4YFP was localized strongly in neuronal cell bodies, dendrites, and axons (supplemental Fig. S5, available at www.jneurosci.org as supplemental material). In addition to prominent fluorescence in the presum-

ably glutamatergic neurons of most thalamic nuclei, we noted α4YFP in the cell bodies of GABAergic neurons of the reticular thalamus (supplemental Fig. S5, available at www.jneurosci.org as supplemental material). In most neocortical areas, neuronal cell bodies contained low α4YFP fluorescence levels (data not shown). However, significant α4YFP fluorescence was detected in diffuse axonal fibers innervating the cortex (data not shown). In the anterior cingulate cortex, two parallel medial bands of α4YFP fluorescence appeared outside the cell body layer (data not shown). α4YFP was also detectable in axonal fibers in the internal capsule (supplemental Fig. S5*G*, available at www.jneurosci.org as supplemental material), which comprise thalamic and cortical fibers.

We used a battery of functional, binding, immunolabeling, and behavioral assays to examine whether inserting YFP in the α4 nAChR subunit altered the function or expression *in vivo*. First, whole-cell patch-clamp recordings were performed on cultured ventral midbrain neurons from both Hom and WT mice. Nicotinic currents were elicited by application of a low (3 μM) and a nearly saturating dose (300 μM) of ACh, using a theta tube attached to a piezoelectric translator. Nicotinic currents were positively identified because the currents were reversibly blocked by the competitive antagonist DHβE (dihydro-β-erythroidine) (1 μM) (supplemental Fig. S2*A*, available at www.jneurosci.org as supplemental material). Furthermore, other receptors and channels were blocked using atropine, TTX, AP-5, CNQX, bicuculline, and MLA. The average nicotinic peak current densities were about the same in WT as in Hom neuronal cultures (supplemental Fig. S2*A*, available at www.jneurosci.org as supplemental material).

Fura-2 imaging and dose–response relationships were performed on cultured ventral midbrain neurons. Various doses of ACh demonstrated nearly identical dose–response relationships of nicotinic responses between WT and Hom neuronal cultures in the presence of receptor and channel blockers that isolated nicotinic responses (supplemental Fig. S2*B*, available at www.jneurosci.org as supplemental material).

The effects of α4YFP expression on measures of nAChR levels and function in preparations from adult mouse brain are illustrated in Figure 2. Maximal response and EC_{50} values for ACh-stimulated $^{86}Rb^+$ efflux measured in thalamus and cortex (data not shown), dopamine release in striatum, and GABA release in hippocampus were similar in α4YFP Hom and Het and WT mice (Fig. 2*A*). Total high-affinity ^{125}I-epibatidine binding as well as the cytisine-sensitive and cytisine-resistant components of these sites in striatum, cortex, thalamus, and hippocampus of Hom and Het α4YFP mice did not differ from that of WT mice (Fig. 2*B*), indicating that the expression of nicotinic binding sites was unaffected by YFP insertion. Consistent with these observations, binding of ^{125}I-mAb299, which specifically labels the α4 subunit (Whiteaker et al., 2006) was unaffected by YFP insertion (Fig. 2*C*).

Previous work showed that α4* nAChRs mediate nicotine-induced antinociception on the hot plate (Marubio et al., 1999; Damaj et al., 2007). WT, α4YFP, and α4 KO (Ross et al., 2000) mice showed similar baseline reaction times to sensing pain on the hot plate. Similar to the previous studies (Marubio et al., 1999; Damaj et al., 2007), we found that α4 KO mice (Ross et al., 2000) are relatively resistant to nicotine-induced antinociception, whereas α4YFP Hom, Het, and WT mice showed similar

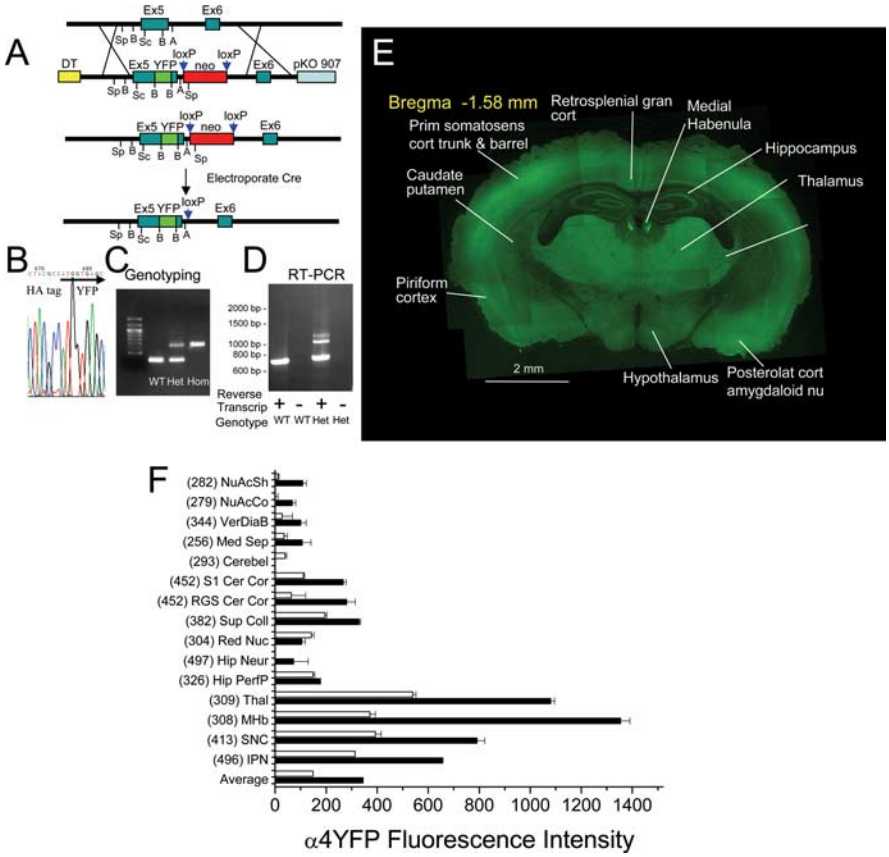

Figure 1. Construction of the α4YFP mouse and whole-brain fluorescence. ***A***, Genomic map of the wild-type mouse α4 nAChR allele located on chromosome 2 (top). Targeting vector was constructed with the α4 gene including exons 5 and 6 and the YFP mutation inserted in the pKO V907 vector (second line; note an inserted HA-epitope tag immediately upstream of YFP is not shown). The neomycin-resistance gene (neo) flanked by loxP sites and the diphtheria toxin A (*DT*) gene were also inserted as positive and negative selection markers. Map of the recombined α4 gene (third line). The neo cassette was deleted by electroporating the neo-intact ES cells with a cytomegalovirus-Cre plasmid to generate neo-deleted ES cell lines (fourth line). Restriction sites: A, *Avr*II; B, *Bst*EII; Sc, *Sac*I; Sp, *Spe*I. ***B***, Chromatogram showing the start of the YFP sequence and the upstream HA-epitope tag in the α4 nAChR gene. ***C***, PCR genotyping of WT, Het, and Hom α4YFP mice. ***D***, RT-PCR showing α4 mRNA expression from combined thalamic–ventral midbrain tissue from Het and WT mice. The higher molecular weight band in the Het is message from the α4YFP allele. Negative controls, lacking reverse transcriptase in the RT-PCR, were devoid of bands. ***E***, Montage of tiled confocal images of a coronal brain section at the hippocampal level from a Hom α4YFP mouse showing overall brain distribution of α4YFP. ***F***, Quantification of α4YFP fluorescence using spectral confocal imaging taken from various brain regions from brain sections of WT, Het, and Hom α4YFP mice. The horizontal bar plots show mean α4YFP intensity (±SEM) for Het and Hom mice for each brain region. Residual autofluorescence intensity from WT mice are shown in brackets and subtracted from the raw intensity values from Het and Hom. CauPut, Caudate–putamen; NuAcSh, nucleus accumbens shell; NuAcCo, nucleus accumbens core; VerDiaB, vertical diagonal band; Med Sep, medial septum; Cerebel, cerebellar cortex; S1 CerCort, primary somatosensory cortex of barrel and trunk; RGS Cer Cor, retrosplenial granular cerebral cortex; Sup Coll, superior colliculus; Red Nuc, red nucleus; Hip Neur, hippocampal interneurons; Hip PerfP, hippocampal medial perforant path; Thal, dorsolateral geniculate nucleus of thalamus; MHb, medial habenula; IPN, interpeduncular nucleus. The "Average" bars show the α4YFP fluorescence averaged for the various regions for both Het and Hom mice.

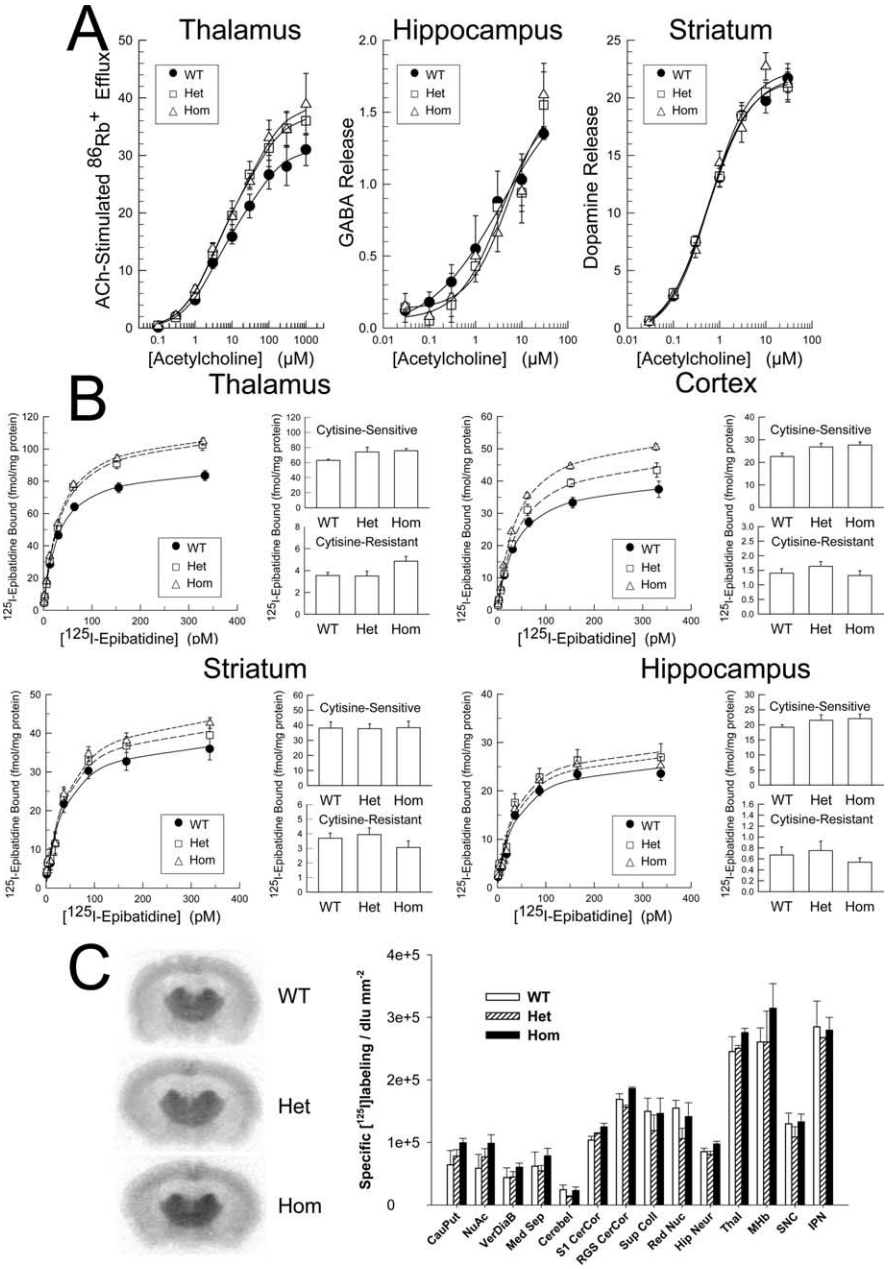

Figure 2. Ion flux, transmitter release, agonist binding, and immunohistochemistry data. ***A***, Left, Dose–response relationships for ACh evoked $^{86}Rb^+$ efflux measurements from synaptosomes made from thalamic tissue from WT, Het, and Hom α4YFP mice. Data were fitted to two (H, L) components. For WT, $EC_{50}H = 2.6 \pm 0.7$ μM, $EC_{50}L = 79 \pm 35$ μM; Het, $EC_{50}H = 3.2 \pm 0.4$ μM, $EC_{50}L = 54 \pm 9$ μM; Hom, $EC_{50}H = 2.8 \pm 2.7$ μM, $EC_{50}L = 75 \pm 110$ μM. Middle, Right: Dose–response relationships of GABA (middle) and dopamine (right) release from the hippocampal and striatal synaptosomes, respectively, from WT, Het, and Hom α4YFP mice. Data were fitted to a single component including a Hill coefficient (*n*). GABA release: WT, $EC_{50} = 3.7 \pm 0.49$ μM, $n = 0.56 \pm 0.25$; Het, $EC_{50} = 3.5 \pm 1.34$ μM, $n = 0.94 \pm 0.29$; Hom, $EC_{50} = 5.1 \pm 1.8$ μM, $n = 1.0 \pm 0.32$. Dopamine release: WT, $EC_{50} = 0.57 \pm 0.09$ μM, $n = 0.93 \pm 0.14$; Het, $EC_{50} = 0.56 \pm 0.05$ μM, $n = 0.97 \pm 0.09$; Hom, $EC_{50} = 0.61 \pm 0.18$ μM, $n = 1.0 \pm 0.29$. ***B***, Concentration dependence of ^{125}I-epibatidine binding in the membrane fraction of thalamus, cortex, striatum, and hippocampus from WT, Het, and Hom α4YFP mice. ^{125}I-Epibatidine binding was performed in the presence and absence of cytisine to determine the cytisine-sensitive and cytisine-resistant sites. The cytisine-sensitive binding sites are likely α4β2 nAChRs. ***C***, Quantitative autoradiography of ^{125}I-mAb 299 labeling in WT, Het, and Hom α4YFP mice. Representative coronal sections are shown at the hippocampal level. Nonspecific labeling was defined in parallel sets of sections from $\alpha4^{-/-}$ mice, and was subtracted from total signal to define regional specific labeling. The histogram shows mean regional specific labeling densities (±SD) for each genotype. Abbreviations are as in Figure 1 *H*.

pharmacological sensitivity to nicotine-induced antinociception (supplemental Fig. S3, available at www.jneurosci.org as supplemental material). In data not shown, we also found that nicotine produces hypothermia equally in α4YFP Hom, Het, and WT mice.

Thus, using electrophysiology, fura-2 imaging, radiolabeled agonist binding, radiolabeled Rb^+ efflux, neurotransmitter release, immunolabeling, and behavioral measurements, we found that α4YFP nAChRs in knock-in mice functioned and expressed like wild-type receptors. These data form the basis for examining changes produced by chronic exposure to nicotine.

Nicotine-induced α4YFP upregulation in midbrain GABAergic neurons

Dopaminergic reward systems include highly nicotine-sensitive neurons in the VTA and SNC (Stolerman and Shoaib, 1991; Mirenowicz and Schultz, 1996; Schultz et al., 1998; Hyman et al., 2006), and an accurate map of high-sensitivity nicotinic receptor expression in this region would further our understanding of the precise actions of nicotine. Therefore we labeled specific neuronal subpopulations within this region using cell-type specific markers, specifically dopaminergic neurons (tyrosine hydroxylase) versus GABAergic neurons (GAD67).

Figure 3 shows images of α4 expression in the ventral midbrain with tyrosine hydroxylase double label for dopaminergic neurons; triple labeling with GAD67 was also performed. The tabulated data (Tables 1, 2) show that nearly all neurons in the SNC are dopaminergic and >99% contain α4, as expected. In the VTA, 90% of neurons are dopaminergic, whereas 10% are GABAergic, as expected (Johnson and North, 1992). Of the GABAergic VTA neurons, ~92% had detectable levels of α4YFP fluorescence (Fig. 4), extending previous data (Yin and French, 2000; Klink et al., 2001; Mansvelder et al., 2002). In the SNR, 99% of the GABAergic neurons contained α4, extending previous data (Klink et al., 2001) (Fig. 4) (described in more detail below). α4YFP fluorescence in dopaminergic neurons of the VTA and SNC had approximately twice the intensity of that found in GABAergic neurons in the SNR (Fig. 3*B–D*); but these data show, for the first time, that nearly all VTA and SNR GABAergic neurons express α4* receptors. α4YFP was also found in dopaminergic and nondopaminergic fibers of the dorsal striatum and was also detectable in dopaminergic fibers innervating the nucleus accumbens (supplemental Fig. S4, available at www.jneurosci.org as supplemental material).

We performed experiments to quantitate the effect of chronic nicotine on α4* receptor levels in α4YFP mice. Nicotine at 2 $mg \cdot kg^{-1} \cdot h^{-1}$ or saline was infused for 10 d via miniosmotic

pumps to α4YFP Hom mice; and α4YFP fluorescence was measured in various brain regions to examine potential changes in α4* nAChR levels (Tables 1, 2). Surprisingly, α4YFP fluorescence did not change significantly from control to nicotine-treated mice in dopaminergic neurons of both SNC (106 ± 2%) and VTA (109 ± 3%). However, GABAergic neurons of both SNR (146 ± 4%) and VTA (136 ± 7%) showed significant ($p < 0.001$ and $p < 0.002$, respectively) increases in α4YFP fluorescence (Tables 1, 2; Fig. 4). With a lower dose of nicotine (0.4 $mg \cdot kg^{-1} \cdot h^{-1}$), there was also a larger increase in α4YFP fluorescence in GABAergic neurons of SNR (117 ± 2%) compared with dopaminergic neurons of VTA (102 ± 4%) and SNC (110 ± 3%) (data not shown). These data in midbrain indicate differential receptor level changes in response to chronic nicotine, specific to neuronal subpopulations.

We acknowledge that the brain slice patch-clamp studies (described below) were performed on mice 30–38 d of age, and the experiments of Tables 1 and 2 on mice 67–69 d of age. To diminish the possibility that these two age groups respond differently to chronic nicotine, we performed pilot experiments on fluorescent imaging in α4YFP mice 42–52 d of age. We observed selective upregulation of α4YFP fluorescence in GABAergic but not dopaminergic neurons, as in Tables 1 and 2.

Chronic nicotine increases firing frequency in GABAergic, but not dopaminergic neurons, in response to acute nicotine

Because it is crucial to investigate the functional state of upregulated receptors, we sought to determine how neuronal signaling changed in these chronically treated circuits. We performed direct electrophysiological experiments on GABAergic compared with dopaminergic neurons in midbrain slices. The electrophysiological criteria for distinguishing dopaminergic versus GABAergic cells in rodent VTA are now uncertain (Ford et al., 2006; Margolis et al., 2006); we therefore studied neurons in the substantia nigra, where the dopaminergic and GABAergic cells occupy distinct subnuclei (SNC and SNR, respectively). We also found that SN neurons maintained their health much better than VTA neurons in slices from young animals that had been implanted for 10 d with osmotic minipumps. The recorded neurons in SNR and SNC did display the respective electrophysiological and pharmacological characteristics thought to distinguish

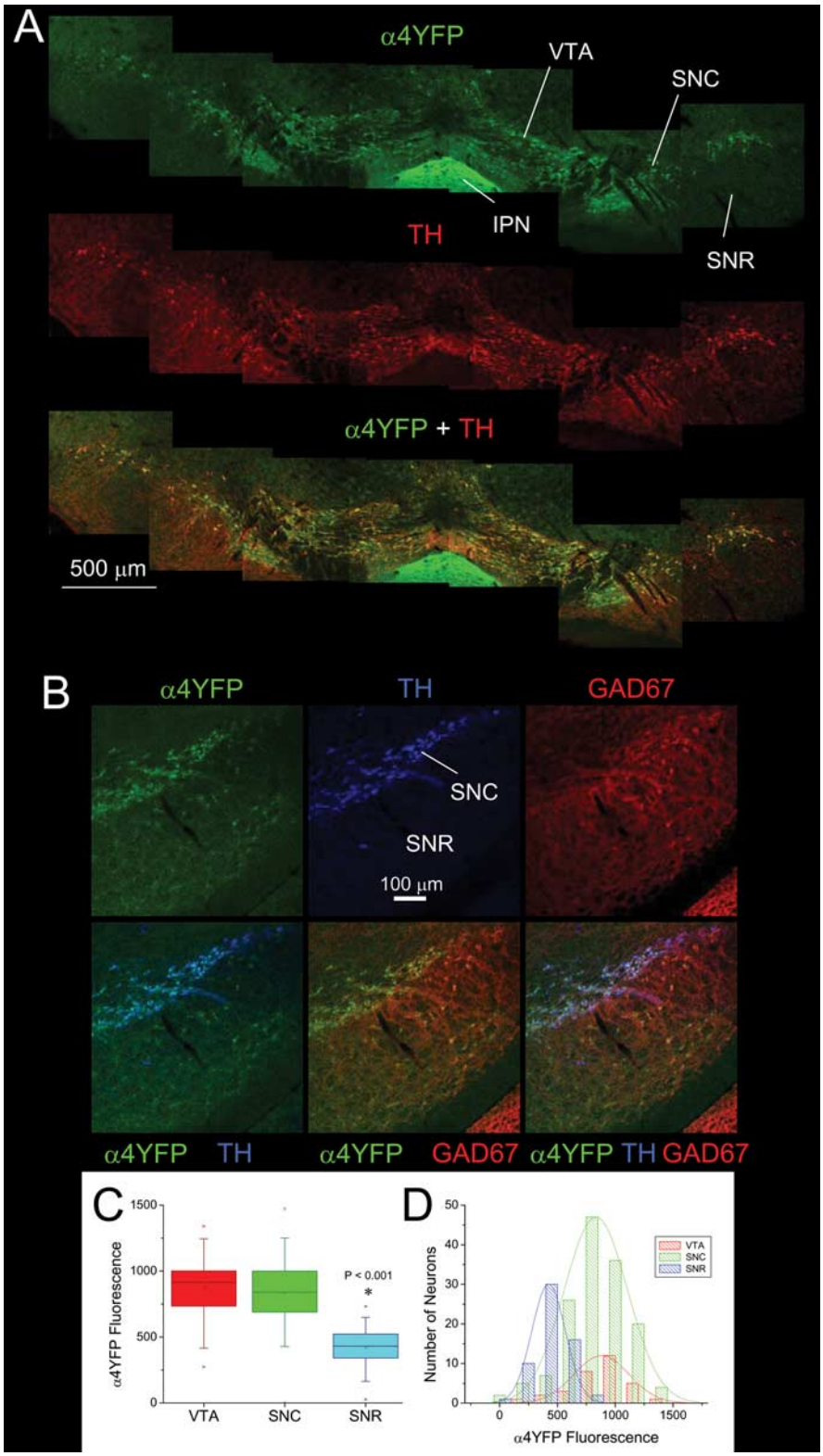

Figure 3. Staining and quantification of dopaminergic and GABAergic α4YFP-containing neurons in the SN and VTA. ***A***, Double labeling showing α4YFP (green) in most TH^+ dopaminergic (red) neurons in the VTA and SNC. Intense α4YFP labeling is found in the interpeduncular nucleus (IPN) and light α4YFP fluorescence is found in the SNR. ***B***, Triple labeling at higher magnification showing strong α4YFP (green) fluorescence in dopaminergic neurons (TH; blue) of the SNC and moderate α4YFP fluorescence in GABAergic neurons (GAD67; red) of the SNR. ***C***, ***D***, Quantification of α4YFP intensities per TH^+ dopaminergic and $GAD67^+$ GABAergic neuron in either the VTA, SNC, or SNR are shown with box plots (***C***) and histogram distributions (***D***).

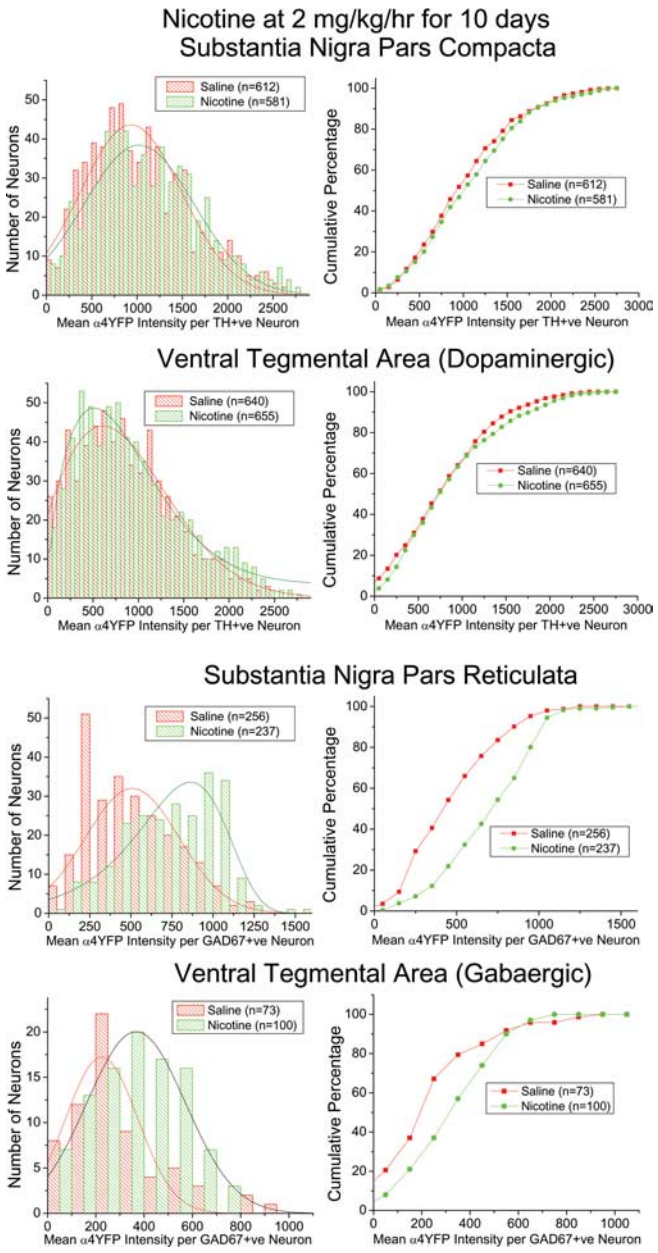

Figure 4. Histograms and cumulative plots showing changes in α4YFP fluorescence in dopaminergic and GABAergic neurons of the SN and VTA with chronic nicotine. Histogram and cumulative plots of the mean α4YFP fluorescence per TH^+ (dopaminergic) or $GAD67^+$ (GABAergic) neuron from α4YFP Hom mice treated either with chronic saline or chronic nicotine ($2\ mg \cdot kg^{-1} \cdot h^{-1}$) for 10 d. α4YFP fluorescence was imaged from VTA, SNC, and SNR from brain sections triple labeled with TH, GAD67, and α4YFP. Dopaminergic neurons in SNC and VTA show very little change in α4YFP. However, GABAergic neurons in VTA and SNR show a shift (increase) in α4YFP intensity with chronic nicotine.

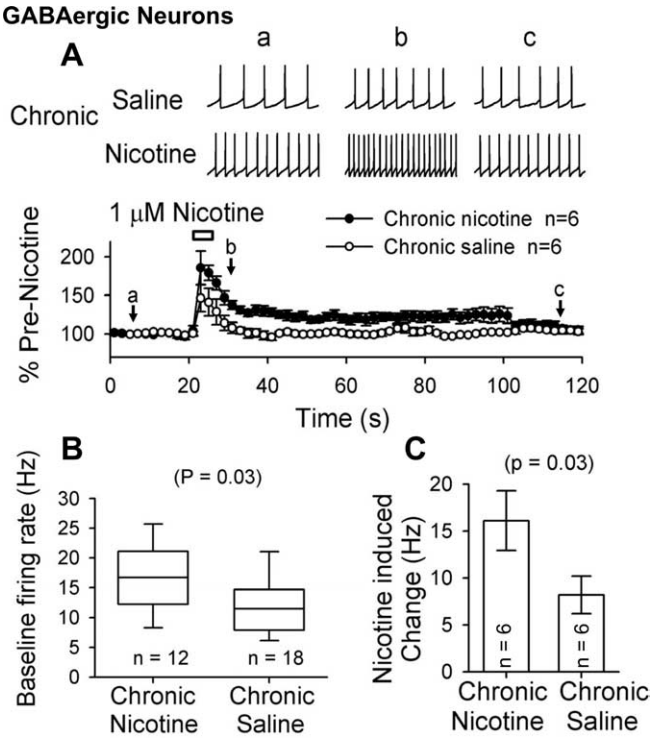

Figure 5. Patch recordings from midbrain GABAergic neurons in slices from mice exposed to chronic nicotine or saline. ***A***, Chronic nicotine treatment enhanced baseline firing rate in SNR GABAergic neurons. Typical traces (0.5 s) (a, baseline; b, peak; c, wash) and time course of firing also show that puff application (5 s) of nicotine (1 μM) increased firing rate in neurons from chronic saline (top traces and empty circles)- and nicotine (bottom traces and filled circles)-treated mice. ***B***, ***C***, Summary of nicotine-induced increment of firing rate in SNR GABAergic neurons. Data in time course and summary are shown as mean ± SEM.

GABAergic and dopaminergic neuron types (i.e., action potential duration, firing frequency, presence of I_h, effects of a μ-opioid agonist, and effects of a dopamine D_2 agonist) (supplemental Fig. S6, available at www.jneurosci.org as supplemental material).

Whole-cell patch-clamp recordings were conducted on ventral midbrain slices prepared from mice (ages, 30–38 d) chronically treated with nicotine for 10 d. Although these mice were younger than those studied in the fluorescence experiments, nAChR receptor levels in rat midbrain dopaminergic areas do not change markedly after day 30 (Azam et al., 2007). In the absence of nicotine, GABAergic neurons from chronically nicotine-treated mice displayed significantly higher baseline firing rates than neurons from chronically saline-treated mice (17.9 ± 1.4 Hz, $n = 12$, vs 12.4 ± 1.7 Hz, $n = 18$; $p = 0.03$) (Fig. 5). This is consistent with the presence of endogenous acetylcholine during the recording, released from the terminals of severed axons of hindbrain cholinergic neurons in the ventral midbrain slice. The inverse was the case for dopaminergic neurons in the absence of acute nicotine. Dopaminergic neurons from chronic nicotine-treated mice had significantly lower basal action potential firing rates than chronic saline-treated mice (1.93 ± 0.17 Hz, $n = 17$, vs 2.64 ± 0.25 Hz, $n = 21$; $p = 0.016$) (Fig. 6*A*,*B*). These data indicate that the functional effects of chronic nicotine correspond to the numerical upregulation observed.

To further test the efficacy of these upregulated receptors, we compared direct nicotine effects in GABAergic neurons from chronically nicotine- or saline-treated mice. When 1 μM nicotine was puffed for 5 s using a picospritzer, GABAergic neurons from chronically nicotine-treated mice also displayed greater increases in peak firing rates than neurons from saline-treated mice (16.1 ± 3.2 Hz, $n = 6$, vs 8.2 ± 2.0 Hz, $n = 6$; $p = 0.03$) (Fig. 5*A*,*C*). These responses were absent in slices perfused with 5 μM mecamylamine (data not shown). Dopaminergic neurons within the SNC are direct downstream synaptic targets of GABAergic neurons within the SNR. Therefore, we sought to address whether alterations in GABAergic firing frequency caused by the presence of upregulated receptors would affect the electrophysiological properties of SNC dopaminergic neurons. To perform this, we bath applied 1 μM nicotine to slices to drive nicotine activation in both GABAergic neurons in the SNR and their

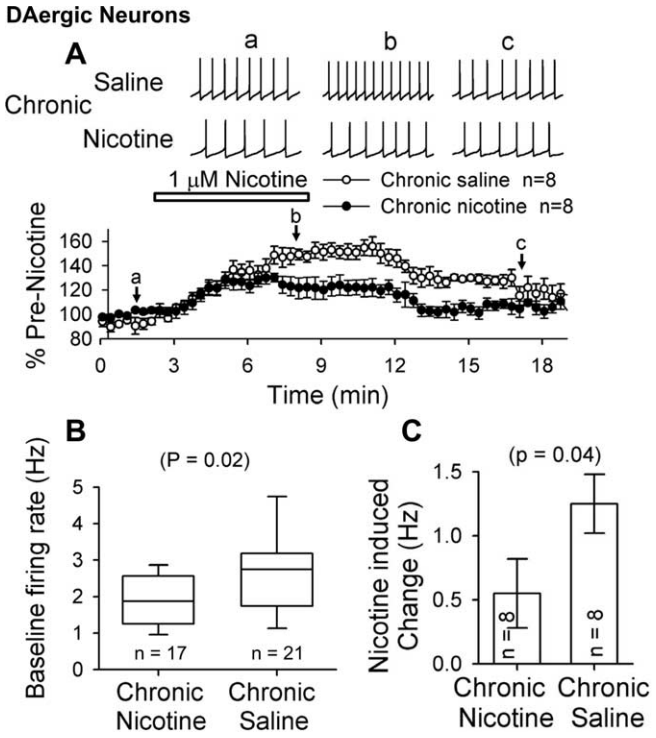

Figure 6. Patch recordings from midbrain dopaminergic neurons in slices from mice exposed to chronic nicotine or saline. ***A***, Chronic nicotine treatment decreased the baseline firing rate of SNC dopaminergic neurons. Typical traces (3 s) and time course of firing also show that nicotine (1 μM) bath perfusion increased firing rate in SNC dopaminergic neurons from chronic saline (empty circles)- and nicotine (filled circles) (a, baseline; b, peak; c, wash)-treated mice. ***B***, ***C***, Summary of nicotine-induced increment of firing rate in SNC dopaminergic neurons. Data in time course and summary are shown as mean ± SEM.

postsynaptic targets, dopaminergic neurons in SNC. In these studies, chronic nicotine plus acute nicotine produced a smaller increase in dopaminergic firing than chronic saline plus acute nicotine (0.55 ± 0.27 Hz, $n = 8$, vs 1.25 ± 0.23 Hz, $n = 8$; $p = 0.04$) (Fig. 6*A*,*C*). Figure 8 provides a schematic explanation for these findings; but in brief, the accelerated firing in the GABAergic neurons and resulting increased inhibition apparently dampened baseline firing in dopaminergic neurons and also blunted the direct excitatory effect of nicotine responses on dopaminergic cells themselves. Therefore, we conclude that chronic nicotine increases both the baseline firing rate and the excitatory effect of 1 μM nicotine in GABAergic neurons, while decreasing baseline firing rate and attenuating the excitatory effect of 1 μM nicotine in dopaminergic neurons. These data suggest that alterations in dopaminergic signaling caused by chronic nicotine could be accounted for by receptor upregulation within GABAergic neurons and that increases in inhibition could provide an explanation for tolerance to the chronic effects of nicotine.

Because dopaminergic neurons in mice chronically exposed to nicotine did not respond vigorously to acutely applied nicotine, one asks whether there is a mechanism imposing a ceiling on nicotine response in dopaminergic neurons. This point should be viewed in light of previous experiments in our laboratory on the dopaminergic neurons of α4Leu9′Ala knock-in mice (Tapper et al., 2004). The Leu9′Ala mice were specifically designed to express hyperactive α4* receptors in place of WT receptors. In dopaminergic neurons from drug-naive Leu9′Ala mice, acutely applied 1 μM nicotine produced significantly greater nicotine responses, and nicotine-induced firing, than in WT mice (Tapper et al., 2004). (Electrophysiological experiments have not been performed on chronic nicotine-treated Leu9′Ala mice.) The data for the Leu9′Ala mice allow one to state that significantly increased α4* sensitivity in dopaminergic neurons can, at least in some cases, result in increased nicotine-induced firing. The apparently unchanged sensitivity in dopaminergic neurons in the present experiments is therefore not likely to result from saturated receptors, unusual spike-generating properties, or unusual cable properties of dopaminergic cells.

α4YFP upregulation in the perforant path of the hippocampus

Fluorescence measurements

α4YFP expression was strong in several glutamatergic fiber tracts innervating the hippocampus: the medial perforant path, the temperoammonic path, and the alveus (Fig. 7*A*). Chronic nicotine produced the largest α4YFP fluorescence increase in the medial perforant path, which contains axons of layer 2 medial entorhinal cortical neurons and is located in the middle one-third of the molecular layer surrounding the dentate granule layer.

After 2 $mg \cdot kg^{-1} \cdot h^{-1}$ nicotine administration for 10 d, the α4YFP fluorescence in the medial perforant path was 94 ± 2% greater than control ($p < 0.001$) (Tables 1, 2). At 0.4 $mg \cdot kg^{-1} \cdot h^{-1}$ nicotine infusion, the increase in α4YFP fluorescence was approximately one-half (44 ± 5%; $p < 0.001$) of that at the higher dose (data not shown), in agreement with previous dose–response data for upregulation of likely α4β2 receptors in mouse brain (Pauly et al., 1991; Marks et al., 2004).

Functional upregulation measured with LTP

LTP, a form of synaptic plasticity related to memory and learning, was discovered in the perforant path (Bliss and Lomo, 1973), and a subsequent study suggests that LTP is induced by acute nicotine in the medial perforant path of nicotine-primed rats (Hamid et al., 1997). We tested whether the increased expression of α4* nAChR and their activation in the medial perforant path can facilitate LTP induction in mouse horizontal hippocampal slices (Fig. 7). We conducted experiments with a presynaptic stimulus intensity (eliciting 40% of the maximum fEPSP slope) (Fig. 7*B*) that did not induce LTP in the absence of nicotine. In slices from chronically nicotine-treated (2 $mg \cdot kg^{-1} \cdot h^{-1}$ for 10–14 d) mice, acute nicotine application (1 μM for 2 min, three times) during tetanic stimulation (100 Hz for 1 s, three times) resulted in robust induction of LTP, because fEPSP slope increased to 131 ± 2% of baseline (Fig. 7*C*). Little or no LTP was found with acute nicotine in slices from mice chronically treated with saline, with slices from both chronic nicotine and chronic saline-treated mice acutely treated with saline (Fig. 7*D*), or with acute application of the noncompetitive antagonist mecamylamine in slices from mice chronically treated with nicotine (the latter resulted in a slight depression of the fEPSC) (data not shown). We also found that, when the stimulus strength was increased to a level that produced 80% of the maximum fEPSP, significant LTP resulted even in the absence of chronic or acute nicotine exposure (data not shown). Thus, activation of the upregulated α4* nicotinic receptors by nicotine lowered the stimulus threshold for LTP induction.

α4YFP upregulation in other areas

Other brain regions showing upregulation of α4YFP fluorescence with chronic nicotine (2 $mg \cdot kg^{-1} \cdot h^{-1}$) included the anterior cingulate cortex (increase of 36 ± 8%), superior colliculus (increase of 34 ± 12%), and the caudate–putamen (increase of 18 ± 4%) (Tables 1, 2). With chronic nicotine administration, there

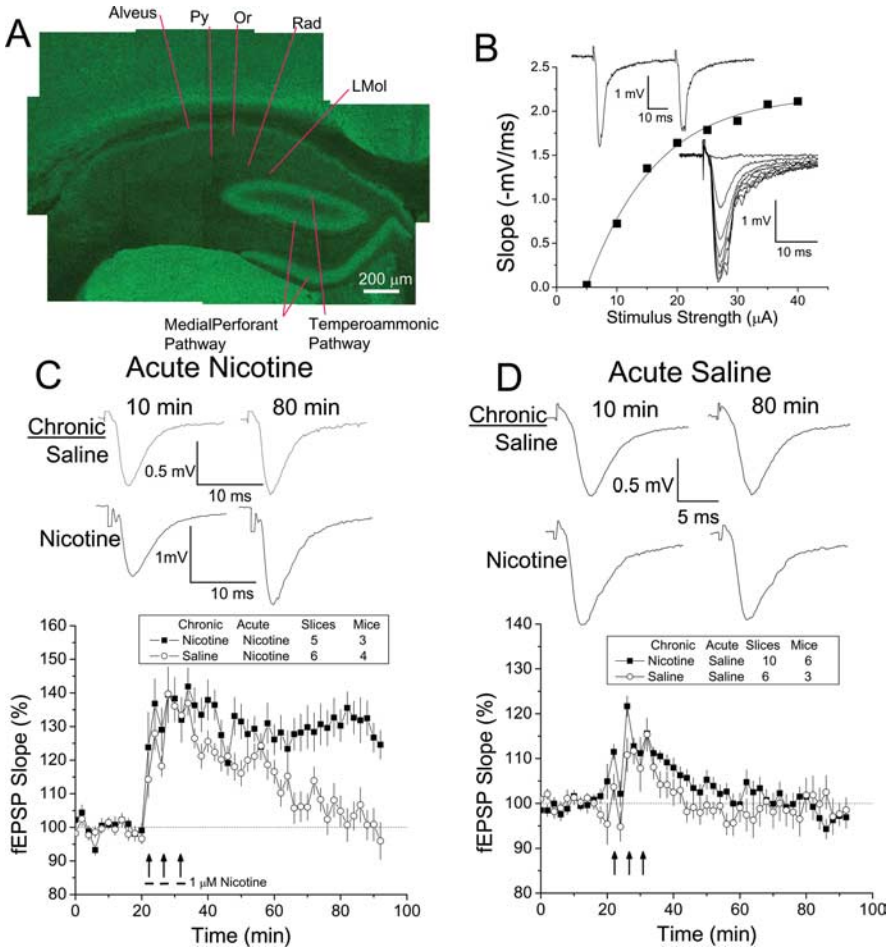

Figure 7. α4YFP in the hippocampus and LTP experiments on the medial perforant path. ***A***, A montage of tiled spectral confocal images of the hippocampus from a Hom α4YFP mouse, showing strong α4YFP fluorescence in axonal fiber tracts including the medial perforant path, the temperoammonic path, and the alveus. Py, Pyramidal cell layer; Or, stratum oriens; Rad, stratum radiatum; L Mol, stratum lacunosum molecular. ***B***, An input–output relationship for fEPSP response slopes. The bottom inset shows the traces with varying stimulus intensities. The stimulus intensity eliciting 40% of the maximal slope was used for baseline stimulus and LTP induction. The top inset shows a paired-pulse stimulation with 50 ms interstimulus interval. The paired-pulse inhibition confirms that stimulation and recording were done in the medial perforant path. ***C***, Traces and plots are shown for fEPSP slope responses on LTP induction recorded from the medial perforant path in hippocampal slices from mice chronically treated with saline or nicotine (2 mg · kg $^{-1}$ · h $^{-1}$ for 10–14 d). Note that fEPSP waveforms are an average of 10 traces. Slices receiving acute nicotine (1 μM) and tetanic stimuli in chronic nicotine-treated mice had larger LTP induction than chronic saline-treated mice. ***D***, Traces and plots of fEPSP slope responses in medial perforant path in hippocampal slices from mice receiving either chronic saline or chronic nicotine. With tetanic stimuli and acute saline, there was no induction of LTP from slices in both chronic saline- and chronic nicotine-treated mice.

was no significant change of α4YFP fluorescence in the dorsolateral geniculate nucleus of the thalamus, the medial habenula, the fasciculus retroflexus, the nucleus accumbens, or the somatosensory area of the cerebral cortex (Tables 1, 2). Interestingly, there was a decrease in α4YFP fluorescence in the interpeduncular nucleus (Tables 1, 2).

Discussion

In the strategy of these experiments, (1) we first constructed a mouse strain with fluorescent α4* receptors. (2) We examined several brain regions for upregulation of fluorescence in response to chronic nicotine. (3) In two cell types showing the strongest upregulation (midbrain GABAergic neurons and axons of the medial perforant path), we performed appropriate physiology to verify functionality of the upregulated receptors. (4) In the dopaminergic neurons that, unexpectedly, showed no numerical upregulation, we confirmed electrophysiologically that there is no functional upregulation.

The relevance of our study depends strongly on experiments associated with step (1). We find that the α4 knock-in mice are quantitatively normal in all respects studied: the regional and cellular pattern of fluorescence (Figs. 1, 3–7; supplemental Fig. S5, available at www.jneurosci.org as supplemental material); nicotine-induced currents (supplemental Fig. S2, available at www.jneurosci.org as supplemental material), Ca^{2+} fluxes (supplemental Fig. S2, available at www.jneurosci.org as supplemental material), $^{86}Rb^{+}$ effluxes (Fig. 2); GABA and dopamine release (Fig. 2); ^{125}I-epibatidine binding (Fig. 2); ^{125}I-mAb299 labeling (Fig. 2); and nicotine-induced antinociception (supplemental Fig. S3, available at www.jneurosci.org as supplemental material). We also point out the good agreement, at the regional level, between the present study of upregulated receptors versus previous studies of upregulated nicotine binding. Indeed, for the nine regions studied with both techniques, the correlation coefficient is 0.91 between percentage upregulation of fluorescence and the percentage upregulation of nicotine binding (Pauly et al., 1991; Marks et al., 1992). Our study also confirms that the previous data on upregulated ligand binding do represent increases in actual nicotinic receptor protein.

Although others have previously found different effects of chronic nicotine among brain areas, in this study the excellent resolution of fluorescence has led to the important fact that α4 upregulation occurs in only a subset of α4-expressing neuronal types. We show here that this cell-specific upregulation provides insights that could resolve the "upregulation dilemma" for α4-dependent processes.

Changes in dopaminergic pathways suggest a mechanism for tolerance

That functional α4* nAChRs are upregulated in GABAergic but not dopaminergic neurons in midbrain by chronic nicotine can, in a general sense, provide mechanisms that lead from upregulated, functional receptors to downregulated release of dopamine (Fig. 8). Our data on GABAergic neurons emphasize cell bodies, consistent with the observation that increased nAChR receptor function from upregulation in inhibitory neurons in the midbrain leads to a corresponding increased basal firing. Our data on midbrain dopaminergic neurons also emphasize cell bodies and lack the resolution to detect possible changes in receptor numbers or function at the presynaptic nerve terminals of dopaminergic axons. However, chronic nicotine also fails to enhance nicotinic stimulation of dopamine release from pinched-off nerve terminals (Grady et al., 1997). Thus, there is little or no

evidence that chronic nicotine upregulates the number or function of highly nicotine-sensitive receptors in dopaminergic neurons.

Although it will probably take some time before all details are known, we provide two exemplary suggestions that use both the present data and the known facts about ventral midbrain circuitry. The first example explains contemporary data on altered accumbal dopamine release in rats recently withdrawn from chronic nicotine (Rahman et al., 2004) (Fig. 8*B*,*C*) (Nisell et al., 1997; Cadoni and Di Chiara, 2000). (1) Endogenous acetylcholine, released from synaptic terminals of cholinergic mesopontine neurons, activates the upregulated receptors, increasing GABAergic neuron firing. This accounts for the data of Figure 5, *A* and *B*. The increased inhibitory firing decreases the firing of the dopaminergic target neurons. This accounts for the data of Figure 6, *A* and *B*, providing a mechanism for dysphoria in the absence of nicotine. (2) During acute nicotine intake, the upregulated receptors increase excitation of the GABAergic neurons; this explains the data of Figure 5, *A* and *C*. This increased firing further inhibits the dopaminergic neurons, partially counteracting their direct excitation by nicotine; this accounts for the data of Figure 6, *A* and *C*. Tolerance to chronic nicotine thus could arise from cell-specific upregulation combined with the sign-inverting properties of a pathway that includes inhibitory neurons.

Another study in rodents showed that chronic nicotine decreased brain reward function as measured by increased threshold of intracranial self-stimulation (Epping-Jordan et al., 1998). The circuits are probably complicated by interneuronal inhibition of GABAergic neurons (Steffensen et al., 1998) and by electrical coupling of GABAergic interneurons (Stobbs et al., 2004). Although other data on midbrain cultures show that chronic nicotine upregulates functional α4* receptors on all the GABAergic neurons (Nashmi et al., 2003; Tapper et al., 2004; Nashmi and Lester, 2007), we caution that the present slice electrophysiology data derive only from substantia nigra recordings.

A conclusion of our study is that upregulation of functional receptors on inhibitory neurons, not desensitization, can explain functional tolerance to nicotine. This view is consistent with a remaining role for desensitization in some aspects of the acute response to nicotine (Mansvelder et al., 2002). In fact, because desensitization occurs with a high probability after channel opening, upregulation may arise more strongly from the desensitized than the activated state of receptors. Conversely, we cannot rule out the idea that each upregulated receptor molecule also features a subtly enhanced functional response to agonists (Vallejo et al., 2005).

We do not yet know whether upregulation of α4* receptors on

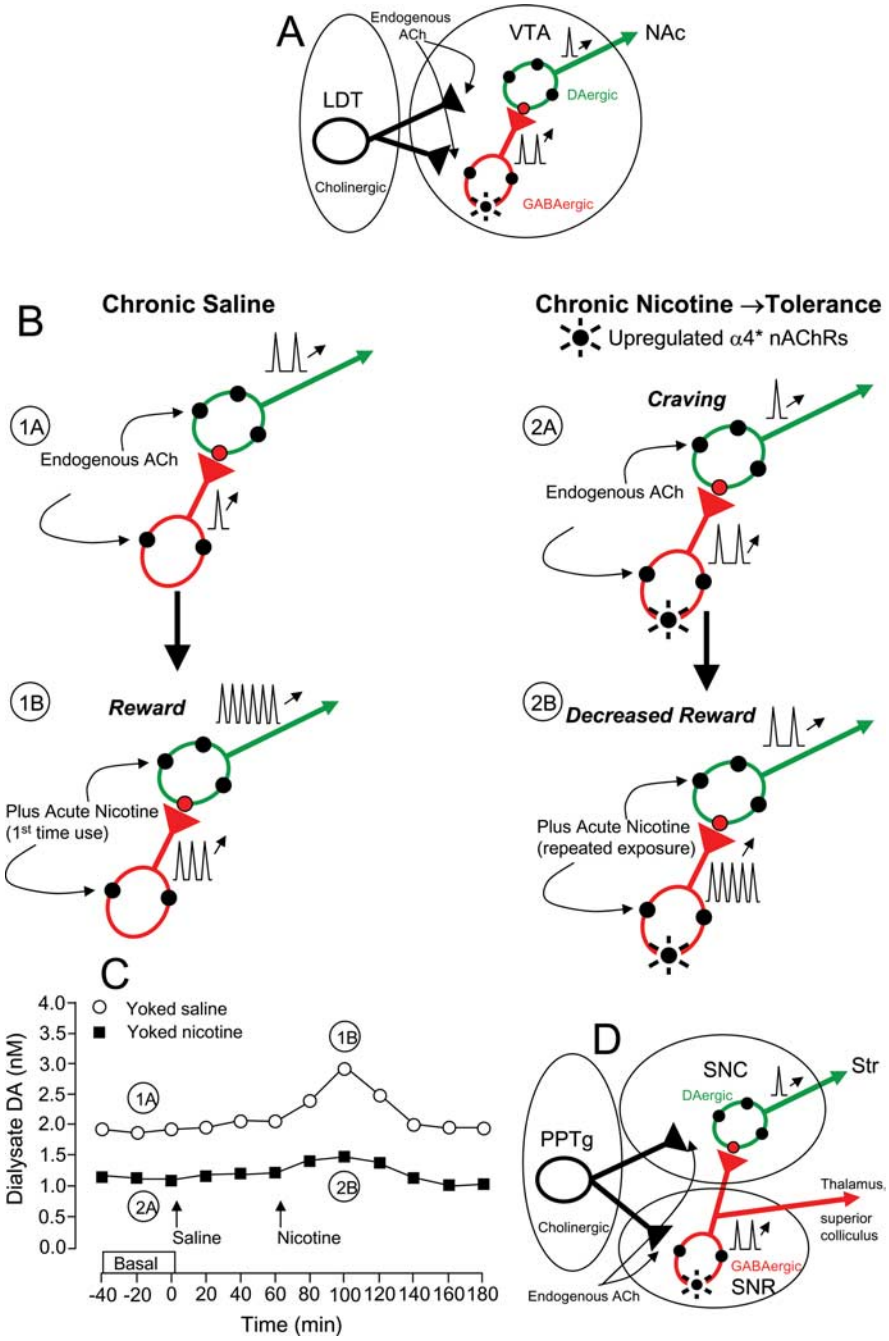

Figure 8. Possible consequences of upregulated functional α4 receptors on midbrain GABAergic neurons. ***A***, Simplified circuit diagram showing the cholinergic lateral tegmental nucleus (LDT) projecting to VTA, in which ~10% of neurons are GABAergic neurons and inhibit the dopaminergic neurons. Both GABAergic and dopaminergic neurons express α4* receptors. The VTA dopaminergic neurons project mainly to the nucleus accumbens. ***B***, ***C***, Events in the nicotine-naive and upregulated VTA, explaining contemporary data from animals yoked to other animals that self-administer nicotine (***C***) (Rahman et al., 2004). In a nicotine-naive animal, endogenous ACh modestly excites GABAergic neurons; and first exposure to nicotine robustly activates dopaminergic neurons ("Yoked saline" in ***C***). After chronic nicotine ("Yoked nicotine" in ***C***), endogenous ACh provides increased inhibitory tone caused by increased α4* receptors in GABAergic neurons. This leads to decreased basal dopamine release, as measured in ***C***. Then, a nicotine dose activates the GABAergic neurons more than previously, blunting activation of the dopaminergic neurons and dopamine release, as measured in ***C***. ***D***, The pedunculopontine tegmental nucleus (PPTg) provides the major cholinergic projection to SN. In SN, the GABAergic and dopaminergic neurons are mostly segregated into SNR and SNC, respectively. As in VTA, both cell types have α4* receptors. SNR neurons have important inhibitory projections to SNC (Mailly et al., 2003) as well as to thalamus and other regions. The events pictured in ***B*** and ***C*** would also apply to SNC.

GABAergic neurons is a general phenomenon that extends outside midbrain; but data from hippocampal interneurons (Alkondon and Albuquerque, 2005) and from GABAergic striatal synapses (Miura et al., 2006) provide additional examples. The present data are not informative with respect to hippocampal interneurons, because we found few if any hippocampal interneurons that express the α4 fluorescence (Fig. 7), as expected from the mixed C57BL/6/129SvJ background of our mice (Gahring et al., 2004).

Possible mechanisms in substantia nigra

In part because we wanted to maintain unambiguous identification of dopaminergic and GABAergic neurons, our slice recordings used substantia nigra, which participates in both reward and the control of movement (Stolerman and Shoaib, 1991; Mirenowicz and Schultz, 1996; Schultz et al., 1998). These results provide our second suggestion that upregulated functional α4* nAChRs could lead to altered dopaminergic function. In substantia nigra of a chronically treated intact animal (Fig. 8*D*), endogenous ACh would also increase (Fig. 5) or regularize SNR GABAergic neuron firing, similar to the suggested benefits of subthalamic nucleus stimulation (Garcia et al., 2005). Via direct SNR to SNC projections (Tepper et al., 1995; Mailly et al., 2003), regularized SNR firing would also decrease firing in SNC dopaminergic neurons (Fig. 6), or specifically decrease burst firing in SNC neurons. This change could protect SNC neurons from excessive activation during any of the several inherited or acquired metabolic conditions that tend to depolarize dopaminergic neurons. In support of this suggested role for α4* receptors, α4 KO mice are less susceptible than WT to protection by nicotine in toxin-induced SN dopaminergic degeneration (Ryan et al., 2001). Such protection provides possible mechanisms for the inverse correlation between smoking and Parkinson's disease (Tanner et al., 2002; Scott et al., 2005; Wirdefeldt et al., 2005).

Sensitization to nicotine at glutamatergic synapses suggests a mechanism for cognitive enhancement

We observed that chronic exposure to nicotine robustly increased α4 fluorescence in the perforant path. In slices from chronically nicotine-treated (but not saline-treated) mice, we then found that acute exposure to nicotine during tetanic stimuli enhances induction of long-term potentiation in the medial perforant path (Fig. 7). Our data on these neocortical glutamatergic neurons emphasize axons, where α4* receptor upregulation presumably arises from enhanced assembly in the soma (Nashmi et al., 2003). Nicotinic activation in axons may result either in increased firing rates or in increased Ca^{2+} influx near presynaptic terminals (MacDermott et al., 1999; Lambe et al., 2003). In this example of nicotine-dependent plasticity, the effect of chronic nicotine thus appears directly explainable by action at a single synapse.

To the extent that LTP of perforant path–dentate gyrus synapses provides an admittedly oversimplified model for some aspects of cognition, nicotine-induced upregulation of α4* receptors in glutamatergic presynaptic structures appears to be a mechanism worth additional investigation in cognitive sensitization by nicotine. These data provide a plausible parallel to reports that, 24 h after withdrawal from nicotine, mice given acute nicotine perform better in a hippocampal-dependent task (Davis et al., 2005) and that chronic nicotine improves spatial working memory in the radial arm maze (Levin et al., 1990, 1996). In the CA1 and CA3 subfield of the hippocampus, chronic nicotine may act via more complex circuit changes (Fujii et al., 1999; Fujii and Sumikawa, 2001; Yamazaki et al., 2006a; Nakauchi et al., 2007).

Chronic nicotine also produced increases in α4YFP fluorescence, presumably in glutamatergic neurons, in the anterior cingulate cortex (increase of 36%), another neocortical region involved in cognition. We also find nicotine-induced upregulation in superior colliculus (increase of 34%), a midbrain nucleus. However, the glutamatergic neurons of the major thalamic nuclei showed no upregulation, in agreement with previous functional data (Nguyen et al., 2004). Chronic exposure to nicotine upregulates functional α4* nAChRs in some but not all glutamatergic neurons.

Mechanism of cell-specific upregulation of α4* receptors

In previous studies on cultured midbrain neurons from WT mice, chronic nicotine upregulated both α4* functional responses and α4* protein levels (Nashmi et al., 2003; Tapper et al., 2004). We also find that upregulation occurs in homotypic GABAergic cultures lacking their typical presynaptic partners and when tested with ACh concentrations that activate only the α4 receptors (Nashmi and Lester, 2007).

Upregulation may arise primarily because more nicotinic receptors are assembled or stabilized in an easily activated state (Nashmi et al., 2003; Darsow et al., 2005; Kuryatov et al., 2005; Sallette et al., 2005; Vallejo et al., 2005). Upregulation of α4β2* receptors appears to depend on specific regions of sequence in the α4 and β2 subunits (Sallette et al., 2004), possibly because these regions allow nicotine to act as a "pharmacological chaperone" (Kuryatov et al., 2005; Sallette et al., 2005). Other data suggest that upregulated receptors have altered functional states, with slower desensitization and enhanced sensitivity to low agonist concentrations (Sallette et al., 2005; Vallejo et al., 2005). Therefore, the cell type-specific upregulation that we observe may itself arise from differences in subunit composition: dopaminergic neurons, but neither GABAergic nor glutamatergic neurons, incorporate α6 subunits into some or all α4* nAChRs (Champtiaux et al., 2003; Salminen et al., 2004; Gotti et al., 2005); and α6* receptors are relatively insensitive to upregulation (Klink et al., 2001; Tumkosit et al., 2006). Cell-specific upregulation could also arise from proteins that govern assembly and trafficking (Keller et al., 2001; Marchand et al., 2002; Darsow et al., 2005; Liu et al., 2005; Sallette et al., 2005; Vallejo et al., 2005; Xu et al., 2006), from mechanisms that regulate receptor turnover (Kuryatov et al., 2005), or from additional factors that regulate desensitization (Mansvelder et al., 2002).

Conclusions

The data meet the challenge presented in Introduction: to find cell types in which α4* receptors are upregulated by chronic nicotine; to test the upregulated receptors for functionality; and to suggest how upregulated, functional receptors can explain two separate effects of chronic nicotine: forebrain-dependent sensitization and midbrain-dependent tolerance. A complete pathophysiological explanation for nicotine addiction must account for several other phenomena such as withdrawal (Koob et al., 2004; Laviolette and van der Kooy, 2004); nor do we claim to have discovered the complete mechanism for the inverse correlation between smoking and Parkinson's disease (Tanner et al., 2002; Scott et al., 2005; Wirdefeldt et al., 2005). Furthermore, our data do not provide a role for reported nicotine-induced adaptations in proteins other than nAChRs (Chang and Berg, 2001; Ferrari et al., 2002; Brunzell et al., 2003; Marrero et al., 2004; Yeom et al., 2005; Marttila et al., 2006; Yamazaki et al., 2006b; Fornari et al.,

2007). Additional nAChR subtypes presumably also play a role in responses to chronic nicotine; perhaps these roles could be investigated in knock-in mice expressing the appropriate fluorescent receptor subunits.

References

Alkondon M, Albuquerque EX (2005) Nicotinic receptor subtypes in rat hippocampal slices are differentially sensitive to desensitization and early in vivo functional up-regulation by nicotine and to block by bupropion. J Pharmacol Exp Ther 313:740–750.

Azam L, Chen Y, Leslie FM (2007) Developmental regulation of nicotinic acetylcholine receptors within midbrain dopamine neurons. Neuroscience 144:1347–1360.

Bliss TV, Lomo T (1973) Long-lasting potentiation of synaptic transmission in the dentate area of the anaesthetized rabbit following stimulation of the perforant path. J Physiol (Lond) 232:331–356.

Brunzell DH, Russell DS, Picciotto MR (2003) In vivo nicotine treatment regulates mesocorticolimbic CREB and ERK signaling in C57BL/6J mice. J Neurochem 84:1431–1441.

Cadoni C, Di Chiara G (2000) Differential changes in accumbens shell and core dopamine in behavioral sensitization to nicotine. Eur J Pharmacol 387:R23–R25.

Champtiaux N, Gotti C, Cordero-Erausquin M, David DJ, Przybylski C, Lena C, Clementi F, Moretti M, Rossi FM, Le Novere N, McIntosh JM, Gardier AM, Changeux JP (2003) Subunit composition of functional nicotinic receptors in dopaminergic neurons investigated with knock-out mice. J Neurosci 23:7820–7829.

Chang KT, Berg DK (2001) Voltage-gated channels block nicotinic regulation of CREB phosphorylation and gene expression in neurons. Neuron 32:855–865.

Chiu CS, Jensen K, Sokolova I, Wang D, Li M, Deshpande P, Davidson N, Mody I, Quick MW, Quake SR, Lester HA (2002) Number, density, and surface/cytoplasmic distribution of GABA transporters at presynaptic structures of knock-in mice carrying GABA transporter subtype 1-green fluorescent protein fusions. J Neurosci 22:10251–10266.

Colino A, Malenka RC (1993) Mechanisms underlying induction of long-term potentiation in rat medial and lateral perforant paths in vitro. J Neurophysiol 69:1150–1159.

Damaj M, Fonck C, Marks M, Deshpande P, Labarca C, Lester H, Collins AC, Martin B (2007) Genetic approaches identify differential roles for α4β2* nicotinic receptors and downstream events in acute models of antinociception in mice J Pharmacol Exp Ther 321:1161–1169.

Dani JA, Bertrand D (2007) Nicotinic acetylcholine receptors and nicotinic cholinergic mechanisms of the central nervous system. Annu Rev Pharmacol Toxicol 47:699–729.

Dani JA, Heinemann S (1996) Molecular and cellular aspects of nicotine abuse. Neuron 16:905–908.

Darsow T, Booker TK, Pina-Crespo JC, Heinemann SF (2005) Exocytic trafficking is required for nicotine-induced up-regulation of α4β2 nicotinic acetylcholine receptors. J Biol Chem 280:18311–18320.

Davis JA, James JR, Siegel SJ, Gould TJ (2005) Withdrawal from chronic nicotine administration impairs contextual fear conditioning in C57BL/6 mice. J Neurosci 25:8708–8713.

de Rover M, Mansvelder HD, Lodder JC, Wardeh G, Schoffelmeer AN, Brussaard AB (2004) Long-lasting nicotinic modulation of GABAergic synaptic transmission in the rat nucleus accumbens associated with behavioural sensitization to amphetamine. Eur J Neurosci 19:2859–2870.

Di Chiara G (2000) Role of dopamine in the behavioural actions of nicotine related to addiction. Eur J Pharmacol 393:295–314.

Dickinson ME, Bearman G, Tilie S, Lansford R, Fraser SE (2001) Multispectral imaging and linear unmixing add a whole new dimension to laser scanning fluorescence microscopy. Biotechniques 31:1272, 1274- 1276, 1278.

Epping-Jordan MP, Watkins SS, Koob GF, Markou A (1998) Dramatic decreases in brain reward function during nicotine withdrawal. Nature 393:76–79.

Ferrari R, Le Novere N, Picciotto MR, Changeux JP, Zoli M (2002) Acute and long-term changes in the mesolimbic dopamine pathway after systemic or local single nicotine injections. Eur J Neurosci 15:1810–1818.

Flores CM, Rogers SW, Pabreza LA, Wolfe BB, Kellar KJ (1992) A subtype of nicotinic cholinergic receptor in rat-brain is composed of α4 subunit and β2-subunit and is up-regulated by chronic nicotine treatment. Mol Pharmacol 41:31–37.

Fonck C, Cohen BN, Nashmi R, Whiteaker P, Wagenaar D, Rodrigues-Pinguet N, Deshpande P, Kwoh S, Munoz J, Labarca C, Collins A, Marks M, Lester H (2005) Novel seizure phenotype and sleep disruptions in knock-in mice with hypersensitive α4 nicotinic receptors. J Neurosci 25:11396–113411.

Ford CP, Mark GP, Williams JT (2006) Properties and opioid inhibition of mesolimbic dopamine neurons vary according to target location. J Neurosci 26:2788–2797.

Fornari A, Pedrazzi P, Lippi G, Picciotto MR, Zoli M, Zini I (2007) Nicotine withdrawal increases body weight, neuropeptide Y and Agouti-related protein expression in the hypothalamus and decreases uncoupling protein-3 expression in the brown adipose tissue in high-fat fed mice. Neurosci Lett 411:72–76.

Fujii S, Sumikawa K (2001) Acute and chronic nicotine exposure reverse age-related declines in the induction of long-term potentiation in the rat hippocampus. Brain Res 894:347–353.

Fujii S, Ji Z, Morita N, Sumikawa K (1999) Acute and chronic nicotine exposure differentially facilitate the induction of LTP. Brain Res 846:137–143.

Gahring LC, Persiyanov K, Dunn D, Weiss R, Meyer EL, Rogers SW (2004) Mouse strain-specific nicotinic acetylcholine receptor expression by inhibitory interneurons and astrocytes in the dorsal hippocampus. J Comp Neurol 468:334–346.

Garcia L, D'Alessandro G, Bioulac B, Hammond C (2005) High-frequency stimulation in Parkinson's disease: more or less? Trends Neurosci 28:209–216.

Gentry CL, Lukas RJ (2002) Regulation of nicotinic acetylcholine receptor numbers and function by chronic nicotine exposure. Curr Drug Targets CNS Neurol Disord 1:359–385.

Gotti C, Moretti M, Clementi F, Riganti L, McIntosh JM, Collins AC, Marks MJ, Whiteaker P (2005) Expression of nigrostriatal α6-containing nicotinic acetylcholine receptors is selectively reduced, but not eliminated, by β3 subunit gene deletion. Mol Pharmacol 67:2007–2015.

Grady SR, Grun EU, Marks MJ, Collins AC (1997) Pharmacological comparison of transient and persistent [^{3}H]dopamine release from mouse striatal synaptosomes and response to chronic L-nicotine treatment. J Pharmacol Exp Ther 282:32–43.

Grady SR, Meinerz NM, Cao J, Reynolds AM, Picciotto MR, Changeux JP, McIntosh JM, Marks MJ, Collins AC (2001) Nicotinic agonists stimulate acetylcholine release from mouse interpeduncular nucleus: a function mediated by a different nAChR than dopamine release from striatum. J Neurochem 76:258–268.

Hamid S, Dawe GS, Gray JA, Stephenson JD (1997) Nicotine induces long-lasting potentiation in the dentate gyrus of nicotine-primed rats. Neurosci Res 29:81–85.

Hyman SE, Malenka RC, Nestler EJ (2006) Neural mechanisms of addiction: the role of reward-related learning and memory. Annu Rev Neurosci 29:565–598.

Johnson SW, North RA (1992) Two types of neurone in the rat ventral tegmental area and their synaptic inputs. J Physiol (Lond) 450:455–468.

Keller SH, Lindstrom J, Ellisman M, Taylor P (2001) Adjacent basic amino acid residues recognized by the COP I complex and ubiquitination govern endoplasmic reticulum to cell surface trafficking of the nicotinic acetylcholine receptor α-subunit. J Biol Chem 276:18384–18391.

Klink R, de Kerchove d'Exaerde A, Zoli M, Changeux JP (2001) Molecular and physiological diversity of nicotinic acetylcholine receptors in the midbrain dopaminergic nuclei. J Neurosci 21:1452–1463.

Koob GF, Ahmed SH, Boutrel B, Chen SA, Kenny PJ, Markou A, O'Dell LE, Parsons LH, Sanna PP (2004) Neurobiological mechanisms in the transition from drug use to drug dependence. Neurosci Biobehav Rev 27:739–749.

Ksir C, Hakan R, Hall Jr DP, Kellar KJ (1985) Exposure to nicotine enhances the behavioral stimulant effect of nicotine and increases binding of [^{3}H]acetylcholine to nicotinic receptors. Neuropharmacology 24:527–531.

Kuryatov A, Luo J, Cooper J, Lindstrom J (2005) Nicotine acts as a pharmacological chaperone to up-regulate human α4β2 acetylcholine receptors. Mol Pharmacol 68:1839–1851.

Labarca C, Schwarz J, Deshpande P, Schwarz S, Nowak MW, Fonck C, Nashmi R, Kofuji P, Dang H, Shi W, Fidan M, Khakh BS, Chen Z, Bowers

BJ, Boulter J, Wehner JM, Lester HA (2001) Point mutant mice with hypersensitive α4 nicotinic receptors show dopaminergic deficits and increased anxiety. Proc Natl Acad Sci USA 98:2786–2791.

Lacey MG, Mercuri NB, North RA (1989) Two cell types in rat substantia nigra zona compacta distinguished by membrane properties and the actions of dopamine and opioids. J Neurosci 9:1233–1241.

Lambe EK, Picciotto MR, Aghajanian GK (2003) Nicotine induces glutamate release from thalamocortical terminals in prefrontal cortex. Neuropsychopharmacology 28:216–225.

Lansford R, Bearman G, Fraser SE (2001) Resolution of multiple green fluorescent protein color variants and dyes using two-photon microscopy and imaging spectroscopy. J Biomed Opt 6:311–318.

Laviolette SR, van der Kooy D (2004) The neurobiology of nicotine addiction: bridging the gap from molecules to behaviour. Nat Rev Neurosci 5:55–65.

Levin ED, Lee C, Rose JE, Reyes A, Ellison G, Jarvik M, Gritz E (1990) Chronic nicotine and withdrawal effects on radial-arm maze performance in rats. Behav Neural Biol 53:269–276.

Levin ED, Kim P, Meray R (1996) Chronic nicotine working and reference memory effects in the 16-arm radial maze: interactions with D1 agonist and antagonist drugs. Psychopharmacology (Berl) 127:25–30.

Liu Z, Tearle AW, Nai Q, Berg DK (2005) Rapid activity-driven SNARE-dependent trafficking of nicotinic receptors on somatic spines. J Neurosci 25:1159–1168.

Luetje CW, Patrick J (1991) Both α- and β-subunits contribute to the agonist sensitivity of neuronal nicotinic acetylcholine receptors. J Neurosci 11:837–845.

MacDermott AB, Role LW, Siegelbaum SA (1999) Presynaptic ionotropic receptors and the control of transmitter release. Annu Rev Neurosci 22:443–485.

Mailly P, Charpier S, Menetrey A, Deniau JM (2003) Three-dimensional organization of the recurrent axon collateral network of the substantia nigra pars reticulata neurons in the rat. J Neurosci 23:5247–5257.

Mansvelder HD, Keath JR, McGehee DS (2002) Synaptic mechanisms underlie nicotine-induced excitability of brain reward areas. Neuron 33:905–919.

Marchand S, Devillers-Thiery A, Pons S, Changeux JP, Cartaud J (2002) Rapsyn escorts the nicotinic acetylcholine receptor along the exocytic pathway via association with lipid rafts. J Neurosci 22:8891–8901.

Margolis EB, Lock H, Hjelmstad GO, Fields HL (2006) The ventral tegmental area revisited: is there an electrophysiological marker for dopaminergic neurons? J Physiol (Lond) 577:907–924.

Marks MJ, Burch JB, Collins AC (1983) Effects of chronic nicotine infusion on tolerance development and nicotinic receptors. J Pharmacol Exp Ther 226:817–825.

Marks MJ, Pauly JR, Gross SD, Deneris ES, Hermans-Borgmeyer I, Heinemann SF, Collins AC (1992) Nicotine binding and nicotinic receptor subunit RNA after chronic nicotine treatment. J Neurosci 12:2765–2784.

Marks MJ, Whiteaker P, Calcaterra J, Stitzel JA, Bullock AE, Grady SR, Picciotto MR, Changeux JP, Collins AC (1999) Two pharmacologically distinct components of nicotinic receptor-mediated rubidium efflux in mouse brain require the β2 subunit. J Pharmacol Exp Ther 289:1090–1103.

Marks MJ, Rowell PP, Cao JZ, Grady SR, McCallum SE, Collins AC (2004) Subsets of acetylcholine-stimulated $^{86}Rb^+$ efflux and [^{125}I]-epibatidine binding sites in C57BL/6 mouse brain are differentially affected by chronic nicotine treatment. Neuropharmacology 46:1141–1157.

Marrero MB, Papke RL, Bhatti BS, Shaw S, Bencherif M (2004) The neuroprotective effect of 2-(3-pyridyl)-1-azabicyclo[3.2.2]nonane (TC-1698), a novel α7 ligand, is prevented through angiotensin II activation of a tyrosine phosphatase. J Pharmacol Exp Ther 309:16–27.

Marttila K, Raattamaa H, Ahtee L (2006) Effects of chronic nicotine administration and its withdrawal on striatal FosB/ΔFosB and c-Fos expression in rats and mice. Neuropharmacology 51:44–51.

Marubio LM, del Mar Arroyo-Jimenez M, Cordero-Erausquin M, Lena C, Le Novere N, de Kerchove d'Exaerde A, Huchet M, Damaj MI, Changeux JP (1999) Reduced antinociception in mice lacking neuronal nicotinic receptor subunits. Nature 398:805–810.

Maskos U, Molles BE, Pons S, Besson M, Guiard BP, Guilloux JP, Evrard A, Cazala P, Cormier A, Mameli-Engvall M, Dufour N, Cloez-Tayarani I, Bemelmans AP, Mallet J, Gardier AM, David V, Faure P, Granon S, Changeux JP (2005) Nicotine reinforcement and cognition restored by targeted expression of nicotinic receptors. Nature 436:103–107.

McCallum SE, Collins AC, Paylor R, Marks MJ (2006) Deletion of the β2 nicotinic acetylcholine receptor subunit alters development of tolerance to nicotine and eliminates receptor upregulation. Psychopharmacology (Berl) 184:314–327.

Mirenowicz J, Schultz W (1996) Preferential activation of midbrain dopamine neurons by appetitive rather than aversive stimuli. Nature 379:449–451.

Miura M, Ishii K, Aosaki T, Sumikawa K (2006) Chronic nicotine treatment increases GABAergic input to striatal neurons. Neuroreport 17:537–540.

Nakauchi S, Yamazaki Y, Sumikawa K (2007) Chronic nicotine exposure affects the normal operation of hippocampal circuits. NeuroReport 18:87–91.

Nashmi R, Lester H (2007) Cell autonomy, receptor autonomy, and thermodynamics in nicotine receptor upregulation. Biochem Pharmacol, in press.

Nashmi R, Dickinson ME, McKinney S, Jareb M, Labarca C, Fraser SE, Lester HA (2003) Assembly of α4β2 nicotinic acetylcholine receptors assessed with functional fluorescently labeled subunits: effects of localization, trafficking, and nicotine-induced upregulation in clonal mammalian cells and in cultured midbrain neurons. J Neurosci 23:11554–11567.

Nashmi R, Fraser SE, Lester H, Dickinson ME (2005) FRET measurements using multispectral imaging. In: Molecular imaging: FRET microscopy and spectroscopy (Periasamy A, Day RN, eds), pp 180–192. New York: Oxford UP.

Nguyen HN, Rasmussen BA, Perry DC (2004) Binding and functional activity of nicotinic cholinergic receptors in selected rat brain regions are increased following long-term but not short-term nicotine treatment. J Neurochem 90:40–49.

Nisell M, Marcus M, Nomikos GG, Svensson TH (1997) Differential effects of acute and chronic nicotine on dopamine output in the core and shell of the rat nucleus accumbens. J Neural Transm 104:1–10.

Pauly JR, Marks MJ, Gross SD, Collins AC (1991) An autoradiographic analysis of cholinergic receptors in mouse brain after chronic nicotine treatment. J Pharmacol Exp Ther 258:1127–1136.

Pauly JR, Marks MJ, Robinson SF, van de Kamp JL, Collins AC (1996) Chronic nicotine and mecamylamine treatment increase brain nicotinic receptor binding without changing α4 or β2 mRNA levels. J Pharmacol Exp Ther 278:361–369.

Paxinos G, Franklin KBJ (2004) The mouse brain in stereotaxic coordinates, Ed 2. Amsterdam: Elsevier Academic.

Picciotto MR, Zoli M, Rimondini R, Lena C, Marubio LM, Pich EM, Fuxe K, Changeux JP (1998) Acetylcholine receptors containing the β2 subunit are involved in the reinforcing properties of nicotine. Nature 391:173–177.

Rahman S, Zhang J, Engleman EA, Corrigall WA (2004) Neuroadaptive changes in the mesoaccumbens dopamine system after chronic nicotine self-administration: a microdialysis study. Neuroscience 129:415–424.

Rezvani AH, Levin ED (2001) Cognitive effects of nicotine. Biol Psychiatry 49:258–267.

Ross SA, Wong JY, Clifford JJ, Kinsella A, Massalas JS, Horne MK, Scheffer IE, Kola I, Waddington JL, Berkovic SF, Drago J (2000) Phenotypic characterization of an α4 neuronal nicotinic acetylcholine receptor subunit knock-out mouse. J Neurosci 20:6431–6441.

Rusted J, Graupner L, Warburton D (1995) Effects of post-trial administration of nicotine on human memory: evaluating the conditions for improving memory. Psychopharmacology (Berl) 119:405–413.

Rusted JM, Warburton DM (1992) Facilitation of memory by post-trial administration of nicotine: evidence for an attentional explanation. Psychopharmacology (Berl) 108:452–455.

Ryan RE, Ross SA, Drago J, Loiacono RE (2001) Dose-related neuroprotective effects of chronic nicotine in 6-hydroxydopamine treated rats, and loss of neuroprotection in alpha4 nicotinic receptor subunit knockout mice. Br J Pharmacol 132:1650–1656.

Sallette J, Bohler S, Benoit P, Soudant M, Pons S, Le Novere N, Changeux JP, Corringer PJ (2004) An extracellular protein microdomain controls upregulation of neuronal nicotinic acetylcholine receptors by nicotine. J Biol Chem 279:18767–18775.

Sallette J, Pons S, Devillers-Thiery A, Soudant M, Prado de Carvalho L, Changeux JP, Corringer PJ (2005) Nicotine upregulates its own receptors through enhanced intracellular maturation. Neuron 46:595–607.

Salminen O, Murphy KL, McIntosh JM, Drago J, Marks MJ, Collins AC, Grady SR (2004) Subunit composition and pharmacology of two classes of striatal presynaptic nicotinic acetylcholine receptors mediating dopamine release in mice. Mol Pharmacol 65:1526–1535.

Schultz W, Tremblay L, Hollerman JR (1998) Reward prediction in primate basal ganglia and frontal cortex. Neuropharmacology 37:421–429.

Schwartz RD, Kellar KJ (1983) Nicotinic cholinergic receptor binding sites in the brain: regulation in vivo. Science 220:214–216.

Scott WK, Zhang F, Stajich JM, Scott BL, Stacy MA, Vance JM (2005) Family-based case-control study of cigarette smoking and Parkinson disease. Neurology 64:442–447.

Steffensen SC, Svingos AL, Pickel VM, Henriksen SJ (1998) Electrophysiological characterization of GABAergic neurons in the ventral tegmental area. J Neurosci 18:8003–8015.

Stobbs SH, Ohran AJ, Lassen MB, Allison DW, Brown JE, Steffensen SC (2004) Ethanol suppression of ventral tegmental area GABA neuron electrical transmission involves *N*-methyl-D-aspartate receptors. J Pharmacol Exp Ther 311:282–289.

Stolerman IP, Shoaib M (1991) The neurobiology of tobacco addiction. Trends Pharmacol Sci 12:467–473.

Swanson LW, Simmons DM, Whiting PJ, Lindstrom J (1987) Immunohistochemical localization of neuronal nicotinic receptors in the rodent central nervous system. J Neurosci 7:3334–3342.

Tanner CM, Goldman SM, Aston DA, Ottman R, Ellenberg J, Mayeux R, Langston JW (2002) Smoking and Parkinson's disease in twins. Neurology 58:581–588.

Tapper A, McKinney S, Nashmi R, Schwarz J, Deshpande P, Labarca C, Whiteaker P, Collins A, Lester H (2004) Nicotine activation of α4* receptors: sufficient for reward, tolerance and sensitization. Science 306:1029–1032.

Tepper JM, Martin LP, Anderson DR (1995) $GABA_A$ receptor-mediated inhibition of rat substantia nigra dopaminergic neurons by pars reticulata projection neurons. J Neurosci 15:3092–3103.

Tumkosit P, Kuryatov A, Luo J, Lindstrom J (2006) β3 subunits promote expression and nicotine-induced up-regulation of human nicotinic α6* nicotinic acetylcholine receptors expressed in transfected cell lines. Mol Pharmacol 70:1358–1368.

Vallejo YF, Buisson B, Bertrand D, Green WN (2005) Chronic nicotine exposure upregulates nicotinic receptors by a novel mechanism. J Neurosci 25:5563–5572.

Waldhoer M, Bartlett SE, Whistler JL (2004) Opioid receptors. Annu Rev Biochem 73:953–990.

Whiteaker P, Peterson CG, Xu W, McIntosh JM, Paylor R, Beaudet AL, Collins AC, Marks MJ (2002) Involvement of the α3 subunit in central nicotinic binding populations. J Neurosci 22:2522–2529.

Whiteaker P, Cooper JF, Salminen O, Marks MJ, McClure-Begley TD, Brown RWB, Collins AC, Lindstrom JM (2006) Immunolabeling demonstrates the interdependence of mouse brain α4 and β2 nicotinic acetylcholine receptor subunit expression. J Comp Neurol 499:1016–1038.

Wirdefeldt K, Gatz M, Pawitan Y, Pedersen NL (2005) Risk and protective factors for Parkinson's disease: a study in Swedish twins. Ann Neurol 57:27–33.

Wooltorton JR, Pidoplichko VI, Broide RS, Dani JA (2003) Differential desensitization and distribution of nicotinic acetylcholine receptor subtypes in midbrain dopamine areas. J Neurosci 23:3176–3185.

Xu J, Zhu Y, Heinemann SF (2006) Identification of sequence motifs that target neuronal nicotinic receptors to dendrites and axons. J Neurosci 26:9780–9793.

Yamazaki Y, Fujii S, Jia Y, Sumikawa K (2006a) Nicotine withdrawal suppresses nicotinic modulation of long-term potentiation induction in the hippocampal CA1 region. Eur J Neurosci 24:2903–2916.

Yamazaki Y, Jia Y, Wong JK, Sumikawa K (2006b) Chronic nicotine-induced switch in Src-family kinase signaling for long-term potentiation induction in hippocampal CA1 pyramidal cells. Eur J Neurosci 24:3271–3284.

Yeom M, Shim I, Lee HJ, Hahm DH (2005) Proteomic analysis of nicotine-associated protein expression in the striatum of repeated nicotine-treated rats. Biochem Biophys Res Commun 326:321–328.

Yin R, French ED (2000) A comparison of the effects of nicotine on dopamine and non-dopamine neurons in the rat ventral tegmental area: an in vitro electrophysiological study. Brain Res Bull 51:507–514.

Yun SH, Park KA, Sullivan P, Pasternak JF, Ladu MJ, Trommer BL (2005) Blockade of nicotinic acetylcholine receptors suppresses hippocampal long-term potentiation in wild-type but not ApoE4 targeted replacement mice. J Neurosci Res 82:771–777.